# PREDICTION OF FAILURE INITIATION OF ADHESIVELY BONDED JOINTS USING MIXED-MODE FRACTURE DATA

A Thesis by

Suranga Gunawardana

B.S., Aerospace Engineering, Wichita State University, 2003

Submitted to the College of Engineering
and the faculty of the Graduate School of
Wichita State University
in partial fulfillment of
the requirements for the degree of
Master of Science

December 2005

**PREDICTION OF FAILURE INITIATION OF ADHESIVELY BONDED JOINTS USING MIXED-MODE FRACTURE DATA**

I have examined the final copy of this Thesis for form and content and recommend that it be accepted in partial fulfillment of the requirement for the degree of Master of Science, with a major in Aerospace Engineering.

_____

Dr. John S. Tomblin, Committee Chair

We have read this thesis
and recommend its acceptance:

_____

Dr. Charles Yang, Committee Member

_____

Dr. Hamid Lankarani, Committee Member

## DEDICATION

To God and my parents

## ACKNOWLEDGEMENTS

I would like to express my sincere appreciation to Dr. John Tomblin, my advisor, for his assistance, advice and concern throughout my graduate experience. I would like to extend my deepest appreciation and gratitude to Waruna Seneviratne, Manager of the Structures Laboratory at the National Institute for Aviation Research (NIAR) for his vision, expertise, patience and enthusiastic guidance throughout the entire project. I would also like to extend my special thanks and appreciation to committee members, Dr. Charles Yang and Dr. Hamid Lankarani for their valuable time and constructive criticism which made this thesis complete.

I would like to thank my family, my father, Justin Gunawardana, my mother, Mallika Gunawardana, my brother, Savinda, and my sister, Mihirani, for always being there for me, encouraging me to pursue my higher educational goals and standing by me through my entire life.. I am also grateful for my friends for their patience, concern and most of all just being there for me when I needed them.

I would also like to thank my fellow employees and managers at NIAR for their assistance at various stages of the project, from layup and fabrication process to testing and analysis. Furthermore I greatly appreciate their help in allocating testing machines and data acquisition equipment to fit my schedule.

Last but not least, I would like to thank NIAR, Industry and State (NIS) for recognizing this project and providing financial assistance as well as materials and equipment, without which this research would not have been possible.

## ABSTRACT

An increased use of adhesively bonded joints in industrial applications has renewed the interest of mixed mode fracture research in adhesive joints. Most practical plane fracture problems are mixed mode, and most advanced materials and joints are shown to fail through mixed mode fracture. It is widely accepted that a useful method for characterizing the toughness of bonded joints is to measure the fracture toughness, $G_C$; energy per unit area needed to produce failure. Mode mixity has a strong dependency toward fracture toughness, and fracture toughness is directly associated with load.

In order to determine the load required to initiate a failure for a given joint configuration, specimens should be fabricated by simulating the original joint and tested followed by an FEM analysis. This process is costly and time consuming. An alternative, simplified method to predict the failure initiation load using mixed-mode fracture toughness data is proposed.

Mode mixity and the corresponding critical strain energy release rate or fracture toughness values are determined for two types of adhesives, Hysol EA 9394 paste adhesive and EA 9628 film adhesive. ASTM and SACMA standardized test methods are used for mode I, II and mixed-mode fracture toughness. Double cantilever beam (DCB) specimens are fabricated with different types of adherends to examine their effect on fracture toughness. Single-lap joint specimens are fabricated for the two adhesive types and tested to determine the actual failure loads, in order to compare the predictions made by the proposed methodology.

FRANC2D is used to model and analyze single-lap joint specimens to determine the mode mixity at failure initiation. Virtual loads are applied to the single-lap joint model to generate load vs. strain energy release rate curves. Failure loads obtained experimentally are then compared with predictions made by the mode-mixity fracture toughness curves for the two adhesive types considered.

It is concluded that failure loads predicted by mixed-mode fracture toughness curves are in good agreement with those obtained experimentally. Recommendations are made for future work in mixed-mode fracture toughness characterization, ranging from process stage to testing methods and analytical tools.

## TABLE OF CONTENTS

## LIST OF TABLES

## LIST OF FIGURES

## LIST OF ABBREVIATIONS

| | |
|---|---|
| ASTM | American Society of Testing and Materials |
| SACMA | Suppliers of Advanced Composite Materials Association |
| PABST | Primary Adhesive Bonded Structure Technology |
| VCCT | Virtual Crack Closure Technique |
| DCB | Double Cantilever Beam |
| SLJ | Single Lap Joint |
| MMB | Mixed Mode Bending |
| ENF | Edge Notched Flexure |
| ELS | End Loaded Split |
| VRMM | Variable Ratio Mixed Mode |
| FRMM | Fixed Ratio Mixed Mode |
| MBT | Modified Beam Theory |
| CLASS | Composite Laminate Analysis Systems |
| AGATE | Advanced General Aviation Transport Experiments |
| NIAR | National Institute for Aviation Research |
| FRANC2D | Fracture Analysis Code 2D |
| CTS | Compression-Tension-Shear |
| PTFE | Poly-Tetra-Fluoro-Ethylene |
| SI | International System |

## LIST OF SYMBOLS

$a$ crack length, in

$a_0$ initial crack length, in

$\tilde{a}$ non-dimensional crack length value

$b$ width of specimen, in

$c$ level length, in

$c_g$ lever length to center of gravity, in

$C$ compliance, $\delta/P$, in/lbf

$E_{11}$ longitudinal modulus of elasticity measured in tension Msi

$E_{22}$ transverse modulus of elasticity, Msi

$E_{1f}$ modulus of elasticity measured in flexure, Msi

$G$ strain energy release rate, kJ/m$^2$

$G_{12}$ shear modulus in plane, Msi

$G_{13}$ shear modulus out of plane, Msi

$G_{\mathrm{I}}$ Mode I component of strain energy release rate, kJ/m$^2$

$G_{\mathrm{II}}$ Mode II component of strain energy release rate, kJ/m$^2$

$G_{\mathrm{C}}$ critical strain energy release rate or fracture toughness, kJ/m$^2$

$h$ half thickness of test specimen, in

$L$ half span length of the mixed mode bending test apparatus, in

$m$ slope of the load vs. displacement curve, lbf/in

$P$ applied load, lbf

$\Delta$ crack length correction for crack tip rotation

$\Gamma$ transverse modulus correction parameter

# CHAPTER 1

# INTRODUCTION

High-performance advanced materials have the ability to stand alongside traditional metals when it comes to material selection for structural design. Innovative designs of composite materials with fibers of carbon, glass, boron, and kevlar with improved matrix materials have become modern engineering materials. Composite materials have become the most popular choice of manufacturers from the consumer products industry to the aerospace industry, replacing aluminum and steel in both secondary and primary structures. The advantages of using composite materials over traditional materials are high strength-to-weight ratio, and significant savings in assembly, inspection, part storage and movement resulting in reliability and low cost.

Traditionally throughout the aircraft industry, part assembly has been done using fasteners, such as rivets and other mechanical means of attachments. This method has caused a dilemma because of the tendency of cracks to occur near fasteners due to effect of stress concentration, thus resulting in low service life. In the 1970s, the United States government together with domestic aircraft manufacturers conducted the analysis of an emerging technology referred to as a “metal bond”. Metal bond technology simply replaced fasteners with adhesives to assemble two or more parts using pressure and high temperature. At the time, due to the lack of knowledge of bonded joint behavior against fatigue, durability, and fracture toughness the aircraft industry was reluctant to pursue this method and limited its use to some secondary part assembly.

The Primary Adhesive Bonded Structure Technology (PABST) [1] program was launched in 1977 to study the behavior of different adhesives relative to fatigue, durability, and fracture toughness. Many new adhesives are still being developed, mostly in the forms of film adhesive and paste adhesive for metal as well as composite material assembly and PABST continues to be relevant to the industry. Manufacturers of the most popular adhesives used in the industry today—Loctite, American Cyanamid Corporation (Cytec) and 3M Corporation—are

contributors to the PABST program. The main advantages of using adhesive over mechanical fastening methods are weight savings and uniform load distribution thus avoiding stress concentration. Other advantages can be listed as follows:

- Reduced number of production parts
- Reduced manufacturing procedures in machining, milling, and riveting
- High strength-to-weight ratio
- Cleaner and smoother finish for aerodynamic benefits
- Less labor
- Low cost
- Higher fatigue resistance
- Damping characteristics and noise reduction compared to mechanical joints
- Allowance for varying coefficients of thermal expansion when joining materials

An increased use of adhesively bonded joints in industrial applications has renewed the need for research in design and analysis of bonded joints, especially in failure prediction. The layered nature of composite adherends and relative weakness in the thickness direction makes the failure mechanism of the joint more complex than that of a traditional metal-to-metal bond [2]. The loading configuration of a bond reflects its failure behavior; hence, failure modes have been categorized accordingly. The literature often refers to loading "modes" when discussing fracture behavior because all loading configurations can be broken down to one or more modes, as shown in Figure 1.1, making it simpler to analyze. Failure of a bonded joint is affected by many other factors in addition to loading configuration. The type of adhesive, cure cycle, environmental effects, and surface preparation are some of the most popular factors. The fracture mechanics approach to analyzing a bonded joint assumes a crack in the joint and studying its behavior under different loading modes. This approach is used by industry to predict the service life of a structure.

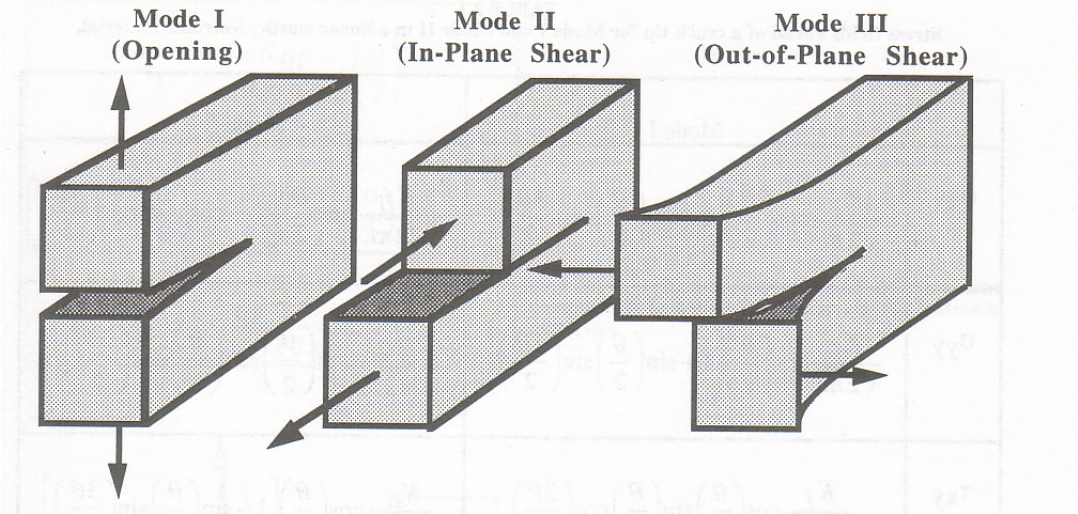


Figure 1.1 Schematic diagrams of failure modes.

## 1.1 Problem Statement

Single- and double-lap shear tests are often used in the industry to determine the strength properties of adhesives in shear by tension loading. ASTM D3165 is particularly intended for this purpose, and the joint closely simulates actual joint configuration of many bonded assemblies. An analysis of the failure mode of these joints reveals the fracture mechanics aspect of the joint. Most practical plane fracture problems are mixed-mode, and most advanced material joints are seen to fail through mixed-mode fracture [3]. It is widely accepted that a useful method for characterizing the toughness of a bonded joint is to measure the fracture toughness, $G_C$; energy per unit area needed to produce the failure. Finite element analysis and other analytical models can be effectively used to calculate the strain energy release rate at failure for an adhesively bonded joint configuration, given the failure load configuration and the material properties.

In order to determine the failure load or stress for a given adhesively bonded joint, usual industry practice requires the fabrication of test specimens that closely simulate the joint

configuration and testing under the appropriate loading configuration until failure. Finite element models need to be developed in order to understand the behavior. This process requires a tremendous amount of resources. A simpler method for estimating the failure load or stress of an initial crack in any adhesively bonded joint for a given adhesive would make the analysis more convenient and benefit the industry as well as the research community.

## 1.2 Objective

Theoretically, fracture toughness values under different loading modes are based on properties of the particular adhesive used in the joint. When calculating the fracture toughness values and embedded mode mixities, the effects of different adherends are yet to be determined. Even with a finite element analysis actual test data is necessary to substantiate the results since different adhesives and adherend combinations may behave differently, especially composite laminate adherends.

The failure mode of a joint is an important factor in the analysis, since it depicts the weaker part of the joint and allows the designers to estimate the problem. Three major failure modes for an adhesively bonded joint are found in literature and often used in the industry, are as follows:

I. **Cohesive Failure**: where internal failure occurs in the adhesive region indicating adhesive strength is less than the strength of the bond (Figure 1.2).

II. **Adhesive Failure**: where failure occurs in the interface between the adherend and the adhesive, indicating improper surface preparation or adhesive type (Figure 1.2).

III. **Adherend Failure**: where failure occurs in the adherend, especially when it is a composite material, indicating that the interlaminar strength of the composite is lower than the adhesive strength (Figure 1.2).

Among these three major failure modes, cohesive failure is interesting because it represents the behavior of the adhesive against fracture as a property. Mode mixity of the crack tip resulted by the stress field is also important since it determines the propagation direction and service life.

The main objective of this investigation is to develop a methodology to predict the failure of a given adhesively bonded joint configuration and to obtain a better understanding of the effects of different adherends and adhesives on the mode-mixity and the fracture toughness relationship. Single-lap joint test per ASTM D3165 standard was selected to confirm the developed methodology.

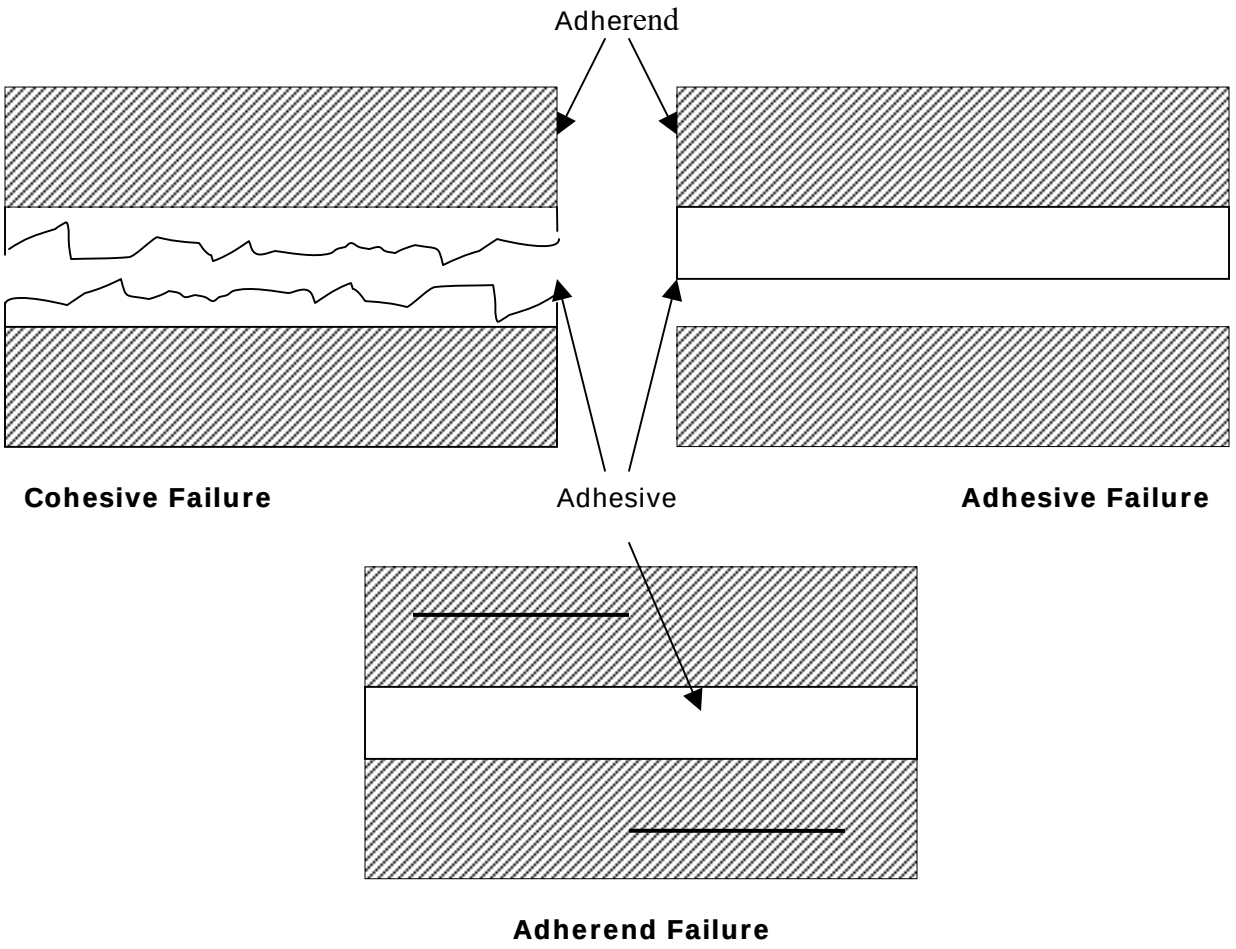


Figure 1.2 Schematic diagrams of failure modes.

## 1.3 Literature Survey

Numerous mixed-mode fracture studies have been conducted over the years, including standardized and non-standardized test methods, analytical models, numerical and computational studies, and the effects of manufacturing procedures on fracture toughness values. Existing standardized tests, such as those from the American Society of Testing Materials (ASTM) and Suppliers of Advanced Composite Materials Association (SACMA), address the interlaminar fracture toughness of fiber-reinforced polymer matrix composites. Similar test methods have been used to obtain fracture toughness values of adhesively bonded joints with minor modifications to specimen configurations and test speeds due to the limited number of standardized test methods dedicated for adhesive joints.

Most analytical models revolve around finite element analysis with different modeling approaches because of its proven accuracy in stress analysis. The state of stress at the crack tip is then related to the strain energy release rate, G, using traditional techniques such as the virtual crack closure technique (VCCT) and J-integral. Modern versions of computational stress analysis packages offer the convenience of bypassing this step and directly solving for strain energy release rates using the above-mentioned theories. However, accuracy of these results depends on models used in predicting the material's behavior. It is difficult to model adhesive behavior for its high non-linearity and vast variety.

Studies have been conducted on the effect of manufacturing variables on fracture toughness values in adhesive joints. It has been found that manufacturing procedures, especially in surface preparation, and environmental conditions can have a substantial effect on these toughness values.

### 1.3.1 Theoretical Work

Weerts and Kossira [5] have studied the mixed mode fracture characterization of adhesive joints on the basis of J-integral using double cantilever beams (DCB) and single-lap joint (SLJ) specimens. The formulation of J-integral is used in a coarsely meshed finite element analysis that bypasses strain singularity and inelastic behavior at the crack tip. Simple determinations of adhesive thickness and near-tip adhesive stresses and strains of a continuum mechanics approach allow mixed-mode characterization. Pirondi and Nicoletto [6] compared various mixed-mode fracture criteria with experimental data using a bonded CTS specimen and a corresponding fixture. Crack propagation in mode I and in mode II were observed to be cohesive at the beginning but developed differently from cohesive to adhesive depending on mode mixity. Nairn [7] emphasized the effect of residual stress consideration in mode I energy release rate evaluation for DCB specimens and adhesives using beam theory, hence avoiding the consequence of ignoring residual stresses, which might have resulted in measuring apparent toughness instead of true toughness. It is also demonstrated that the error between apparent toughness and true toughness can be large and is often larger than the correction required for crack tip rotation effects.

Williams and Moore [8] introduced a protocol to provide guidance on the measurement of peel strength of the laminate and to show how adhesive fracture toughness can be determined from peel strength. Yang et al. [9] numerically studied an elastic-plastic mode II fracture of adhesive joints. A traction-separation law was used to simulate the mode II interfacial fracture of adhesively bonded edge notched flexure specimens loaded in three-point bending. A shell/3D modeling technique was developed by Krueger [10], where a local solid finite element model was used only in the immediate vicinity of the delamination front, combining the accuracy of the full three-dimensional solution with the computational efficiency of a plate or shell finite element model.

### 1.3.2 Experimental Work

The ASTM standard for "Mixed Mode I-Mode II Interlaminar Fracture Toughness of Unidirectional Fiber Reinforced Polymer Matrix Composites" suggests the Mixed-Mode Bending (MMB) test to determine the fracture toughness, $G_C$, of continuous fiber-fiber reinforced composite materials at various mode I to mode II loading ratios [12]; and it is the only standard available to determine fracture toughness in a mixed-mode condition. Hashemi et al. [13] used a variety of test specimens and methods to suggest that partitioning of G on a global energy basis as opposed to using local stress-field solutions is the most appropriate for laminates. A pure mode I double cantilever beam (DCB) specimen, a pure mode II end-loaded split (ELS) specimen, a variable ratio mixed-mode (VRMM) specimen, and a fixed-ratio mixed-mode (FRMM) specimen have been used with the appropriate loading arrangement in this regard. Ramaswamy at el. [4] have studied the mixed-mode crack deformation using a modified flexural specimen and a coherent gradient sensing system. Crack tip parameters, such as stress intensity factor, mode mixity, and energy release rates, have been measured from interference patterns and found to be in good agreement with those determined from theoretical predictions using mode partition based on moment decomposition.

Bardis and Kedward [11] addressed the significance of surface preparation on the long-term durability of bonded composite joints. The effects of release fabric usage and grit blasting on the fracture toughness were evaluated using a composite version of a wedge test, used in quality and durability assessment of metal bonded systems. It was demonstrated that curing nylon release fabrics against adherend surfaces leads to interfacial failures and intermittent crack propagation with reduced loads and crack opening displacements, giving critical stain energy release rates, $G_{IC}$, lower than bonds produced with equivalent PTFE vacuum bag surfaces. Grit-blasted adherends were shown to have higher failure loads and $G_{IC}$ values than non-blasted ones, although the failure mode was not changed.

# CHAPTER 2

# MIXED-MODE FRACTURE TOUGHNESS TESTING

The fracture behavior of a material for a given mode is studied by developing a resistant curve that can be used to predict the load required for propagation. The resistance curve, or R curve, is traditionally the strain energy release rate, G, plotted against the crack extension for a given material. The R curve depicts a basic description of how a fracture behaves in a particular material, since it is the energy needed for a crack to extend. Furthermore, an R curve can predict the stable/unstable regions of the propagation by plotting the driving force against crack length over the R curve, as shown in Figure 2.1 [14].

The R curves for two types of materials are shown. The first case (Figure 2.1a) is a material with a flat curve, indicating constant resistance with crack propagation. The crack remains stable for the first stress level and becomes unstable as the driving force increases but the resistance remains constant. The second case (Figure 2.2a) is a material with a rising curve where crack grows in small extensions with increasing stress level until it reaches a certain point and then becomes unstable as the rate of change in the driving force exceeds the slope of the R curve.

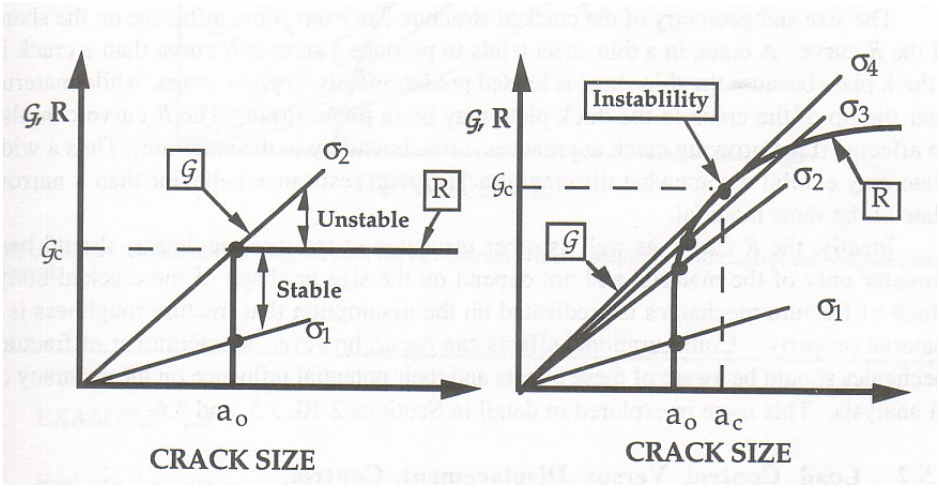


(a) Flat R curve (b) Rising R curve

Figure 2.1 Schematic diagrams of driving force/R curve.

## 2.1 Background

The strain energy release rate of a certain material under a given loading condition can be broken down into three main loading configurations and corresponding strain energy release rate fractions as shown in Figure 1.1. This investigation is limited to mode I, mode II and mixed-mode I and II loading configurations, hence, the total strain energy release rate consists of mode I strain energy release rate $G_I$ and mode II strain energy release rate $G_{II}$.

A mixed-mode R curve would depict the crack propagation of a material under mixed-mode loading conditions. However, this requires a three-dimensional plot and a massive amount of experimental test data which is beyond the scope of this study. Instead, a mode-mixity fracture toughness curve is considered in this investigation, addressing only the fracture initiation of a given crack length. Mode mixity has been noted in the literature as a percentage of the strain energy release rate value corresponding to the mode II portion of the load over the total strain energy release rate, $G_T$ which is used in this study as shown in Equation 2.1. Therefore 0% mode-mixity corresponds to the pure mode I and 100% mode-mixity corresponds to pure mode II loading condition.

$$G_{II}\% = \frac{G_{II}}{G_I + G_{II}} = \frac{G_{II}}{G_T} \tag{2.1}$$

In order to develop a mixed-mode fracture toughness curve for a particular material, the fracture toughness or critical strain energy release rate, $G_C$, needs to be determined at each mode-mixity point, ranging from pure mode I or 0% mode-mixity, to pure mode II, or 100% mode-mixity. It should be noted that the strain energy release rate that is necessary to propagate a crack is referred to as the critical strain energy release rate or fracture toughness, hence, used in plotting the mode-mixity fracture toughness curve. Numerous techniques are available to determine fracture toughness for a given mode. ASTM and SACMA standardized test methods are used in this investigation.

### 2.1.1 Mode I

ASTM recommends D5528 standard for mode I interlaminar fracture toughness. Although this test method is meant for interlaminar fracture toughness of unidirectional composite laminates, it can also be used for adhesive-bonded joints [15]. Specimen configuration is similar to what the standard suggests. The double cantilever beam (DCB) with piano hinges, as shown in Figure 2.2, consists of two adherends bonded with adhesive.

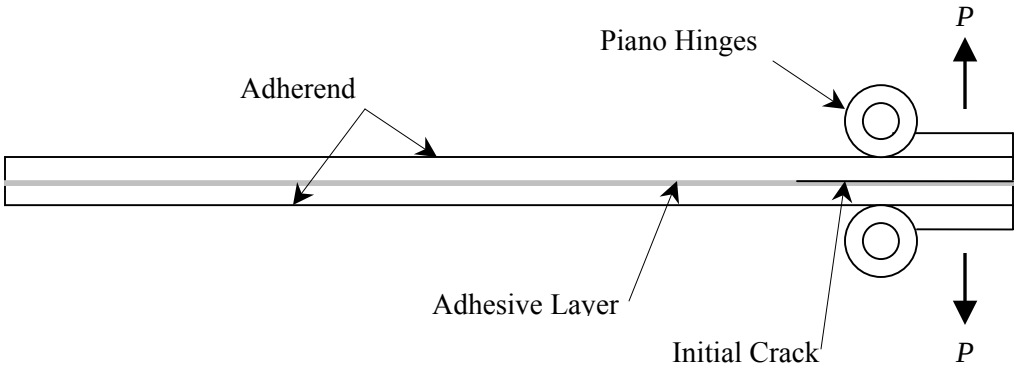


Figure 2.2a Schematic diagram of mode I DCB specimen (side view).

The mode I critical strain energy release rate, $G_{IC}$, was determined using the modified beam theory (MBT), which accounts for rotation at the delamination front, as recommended in ASTM D5528 standard. The final data reduction formula is shown in Equation 2.2. An initial crack length of two inches is recommended.

$$G_I = \frac{3P\delta}{2b(a+|\Delta|)} \tag{2.2}$$

where:

$P$ = Load

$\delta$ = Load point displacement

$b$ = Specimen width

$a$ = Crack length

$\Delta$ = Correction factor for rotation

**Determination of Correction Factor for Rotation, $|\Delta|$ [15]**

As the specimen is loaded in a mode I (opening) loading configuration, as shown in Figure 2.2, the adherend arms tend to rotate due to bending, thus changing the effective crack length. Hence, a correction factor for rotation is introduced into the equation. In order to determine this correction factor, $|\Delta|$, propagation test data points in the load, displacement, and propagation length are required. By plotting load vs. displacement, compliance is calculated for each crack-length propagation. Then the compliance value to the power 1/3 is plotted against crack length ($C^{1/3}$ vs. a) for each propagation, forming a least square plot. The value of the x-axis where the curve crosses the x-axis is the correction factor for rotation, $|\Delta|$. Figure 2.2a illustrates this step with an example.

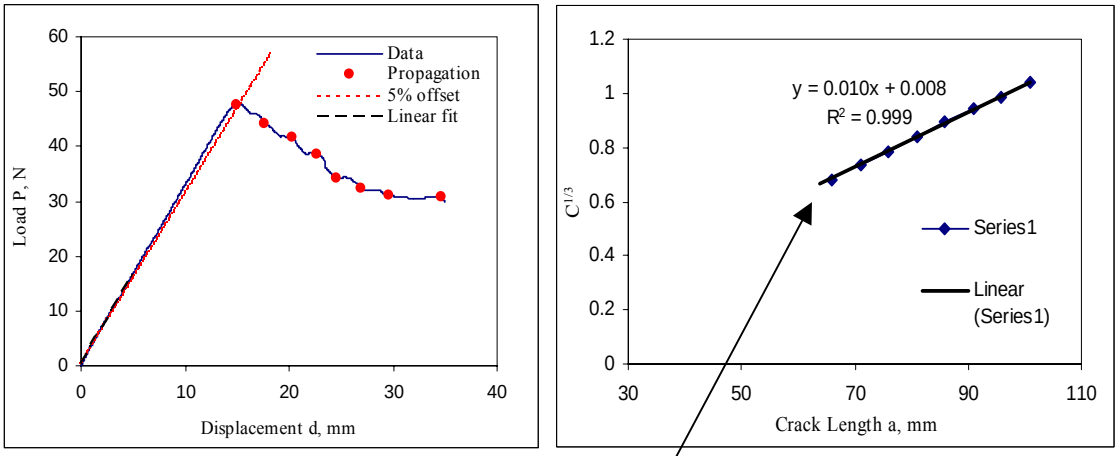


Example:

$$y = 0.01x + 0.008$$

$$y = 0;$$

$$x = 0.8 = \Delta$$

Figure 2.2b Determination of correction factor for rotation, $|\Delta|$.

### 2.1.2 Mode II

SACMA recommends a three-point bend test for mode II interlaminar fracture toughness using an edge notch flexure (ENF) specimen [16]. This standard can also be used effectively for bonded joints. The specimen configuration is similar to what is suggested in the standard, a double cantilever beam (DCB) with two adherends bonded with an initial crack 1.5 inches, as shown in Figure 2.3. As recommended, the mode II critical strain energy release rate, $G_{IIC}$, is determined using the formula shown in Equation 2.3.

$$G_{II} = \frac{9a^2 p^2 C}{2W(2L^3 + 3a^3)} \tag{2.3}$$

where:

$a$ = Crack length

$P$ = Critical load

$C$ = Compliance

$W$ = Specimen width

$L$ = Half length of loading span

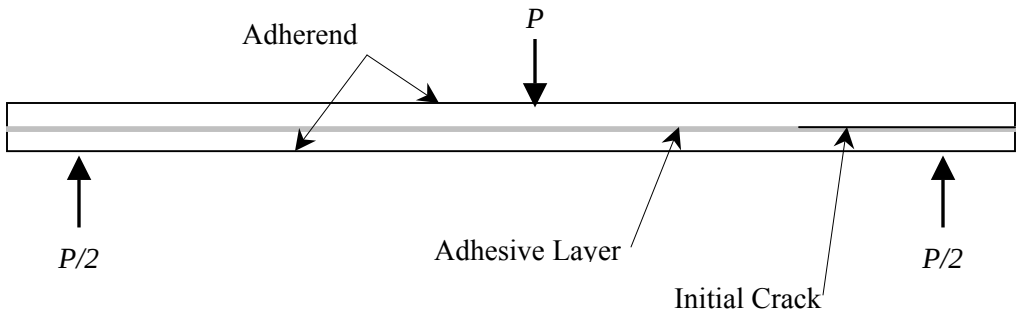


Figure 2.3 Schematic diagram of mode II ENF specimen.

### 2.1.3 Mixed Mode

ASTM recommends standard D6671 for mixed-mode interlaminar fracture toughness of unidirectional composite laminates with the use of a mixed-mode bending technique [12]. The mixed-mode bending technique has been effectively used with adhesively bonded joints as well. The specimen configuration is the same as for mode I as shown in Figure 2.2, except that the initial crack length decreased from two inches to one inch. $G_I$ and $G_{II}$ values are calculated separately using Equations 2.4 and 2.5.

$$G_I = \frac{12P^2(3c-L)^2}{16b^2h^3L^2E_{1f}}(a+\chi h)^2 \tag{2.4}$$

$$G_{II} = \frac{9P^2(c+L)^2}{16b^2h^3L^2E_{1f}}(a+0.43\chi h)^2 \tag{2.5}$$

where:

$$\chi = \sqrt{\frac{E_{11}}{11G_{13}}\left\{3-2\left(\frac{\Gamma}{1+\Gamma}\right)^2\right\}} \qquad \Gamma = 1.18\frac{\sqrt{E_{11}E_{22}}}{G_{13}} \qquad \tilde{a} = \frac{a}{h\chi}$$

$$c = \left(0.167+0.000137\tilde{a}-0.108\sqrt{\ln(\tilde{a})}\left(\frac{G_{II}}{G}\right)^4+\frac{-1400+0.725\tilde{a}^2-141\ln(\tilde{a})-302\ln\left(\frac{G_{II}}{G}\right)}{219-5000\frac{G_{II}}{G}+55\ln(\tilde{a})}\right)L$$

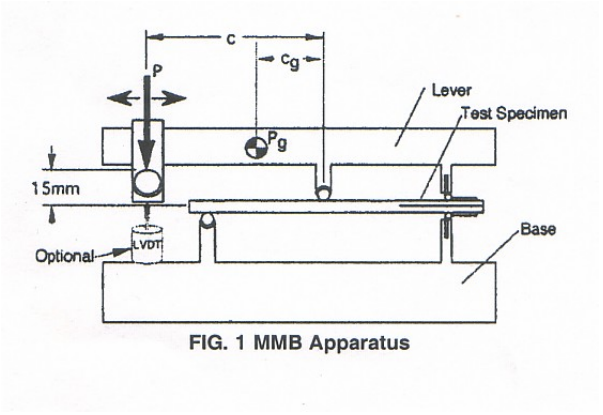


Figure 2.4 Schematic diagram of the mixed mode bending loading [12].

## 2.2 Panel Fabrication and Bonding

This section addresses panel fabrication and bonding, required to fabricate test specimens necessary to generate mode-mixity fracture toughness curves. Panel fabrication involves material selection, adhesive selection, surface preparation, and bonding procedures including cure cycles. This may be the most important step of the entire investigation, since it directly affects the test results. Material and adhesive selection may be approached with a sense of an actual adhesive joint that is useful to the industry. Surface preparation effects on adhesive joint behavior have been investigated previously especially on fracture toughness, and mentioned in the literature survey section [11].

The bonding procedure may change with the type of adhesive used according to the manufacturer recommendations. The cure cycle used for bonding may affect the toughness of the joint. A room temperature-cured adhesive joint may not behave the same as an elevated temperature-cured joint. With so many techniques and procedures available, it is important to be consistent with the fabrication process so that the results obtained are valid for comparison. Some of the key factors in the panel fabrication and bonding process that could affect the final results are listed here:

- Adherend properties (material, layup, thickness, etc.)
- Adherend preparation (layup process, cure cycle, surface roughness, etc.)
- Adhesive properties (adhesive type, bulk adhesive properties, etc.)
- Adhesive preparation (accuracy of mixing ratios, environmental conditions, etc.)
- Bonding method (bond line thickness control, environmental conditions, etc)
- Cure cycle (curing technique, accuracy of apparatus, environmental conditions, etc.)

### 2.2.1 Material Selection and Cure-Cycle

Materials were selected based on the most common single-lap shear test specimens used in the industry. Although it is most common to use aluminum adherends as single-lap shear test specimens to simulate adhesive-bonded joints in shear, the current trend toward composite-adhesive joints led this investigation to select carbon fiber and glass fiber materials. However, anodized aluminum 2024-T3 was also used with the composite adherends to fabricate specimens, in order to understand the effect of adherend material. Resin pre-impregnated materials, better known as prepregs, were used to make adherend panels because of their wide use, availability, and convenience. Three types of adherends were used in this investigation: one with a carbon fiber unitape and fabric combination, a glass fabric, and aluminum. Basic information about the prepreg materials used in adherends is listed in Table 2.1.

Table 2.1 Basic prepreg material information.

| Manufacturer | Fiber Product ID | Resin Product ID | Material Identification |
|---|---|---|---|
| Toray | T700GC-12K-31E | #2510 | Carbon/Epoxy Unidirectional Tape |
| Toray | T700SC-12K-50C | #2510 | Carbon/Epoxy Plain Weave Fabric |
| Newport | 7781 | NB321 | E-Glass/Epoxy Fabric |

Once the material is selected, the next step is to determine the panel geometry and the layup sequence according to the adherend thickness required. Panel geometry was determined to be 18 inch square since the tools available for layup were able to cure a maximum panel of this size conveniently. Layup sequences were determined by the adherend thickness used in the industry for single-lap shear coupons. Although the ply orientations in both adherend layup sequences were the same, the number of plies was determined to maintain an equal adherend thickness. The vacuum bag curing technique using an autoclave was chosen for the adherend panels, since it is the most common and effective way to fabricate panels out of prepreg materials.

**Carbon Adherend**

The layup details for carbon adherends are as follows:

Table 2.2a Carbon adherend layup

| Material Type | Layup | Nominal Thickness |
|---|---|---|
| Carbon/Epoxy Unitape (U) & Plain Weave (PW) | $0_{PW}/[0_U]_8/0_{PW}$ | 0.0652 in |

The cure-cycle for carbon adherends are as follows:

- Ramp 4.5 $^0$F/min to 355 $^0$F
- Constant 355 $^0$F at 85 psi and 5 in-Hg vacuum for 130 min.
- Ramp down 5 $^0$F/min to room temperature

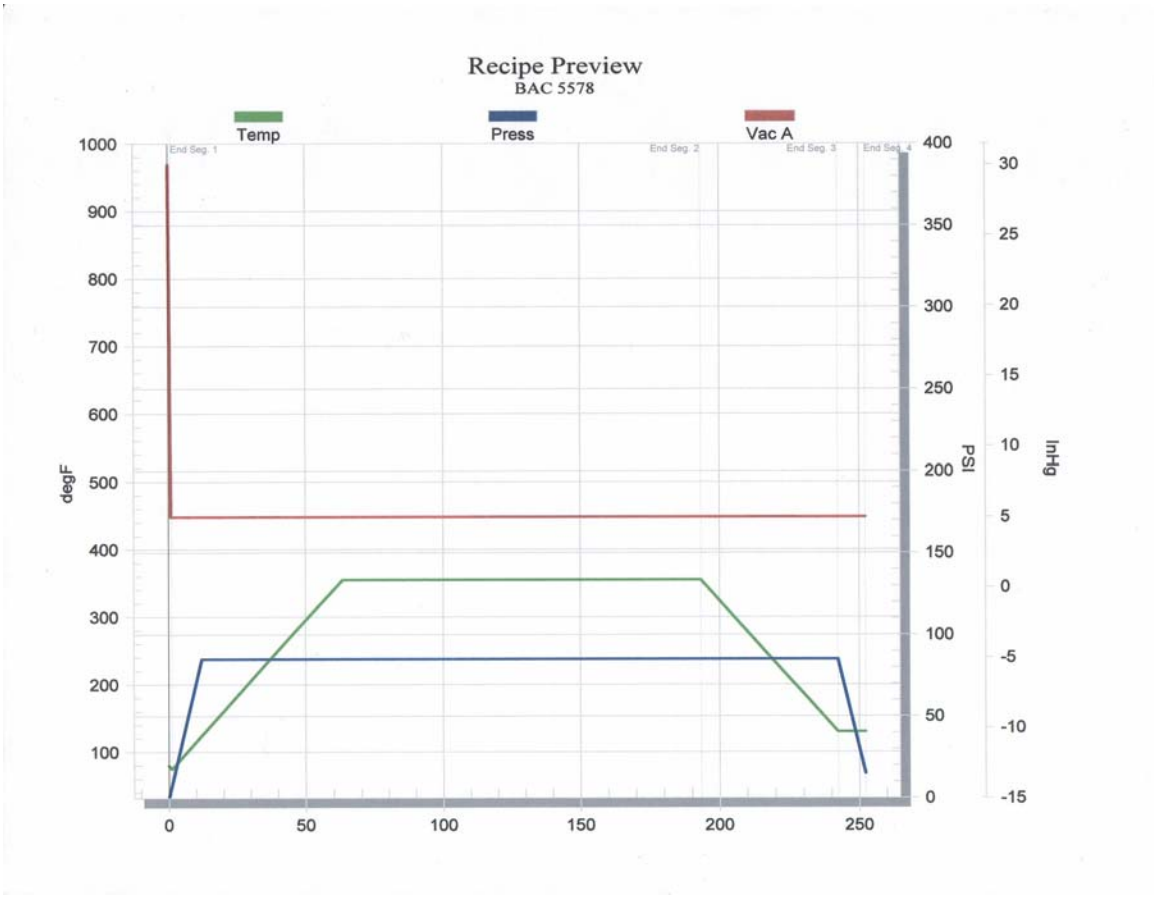


Figure 2.5a Cure cycle report for carbon adherend generated by auto clave.

**Glass Adherend**

The layup details for glass adherends are as follows:

Table 2.2b Glass adherend layup.

| Material Type | Layup | Nominal Thickness |
|---|---|---|
| Glass/Epoxy Fabric (F) | $[0_F]_6$ | 0.0588 in |

The cure-cycle for glass adherends are as follows:

- Ramp 4.5 $^0$F/min to 275 $^0$F
- Constant 275 $^0$F at 0 psi and 30 in-Hg vacuum for 90 min.
- Ramp down 5 $^0$F/min to room temperature

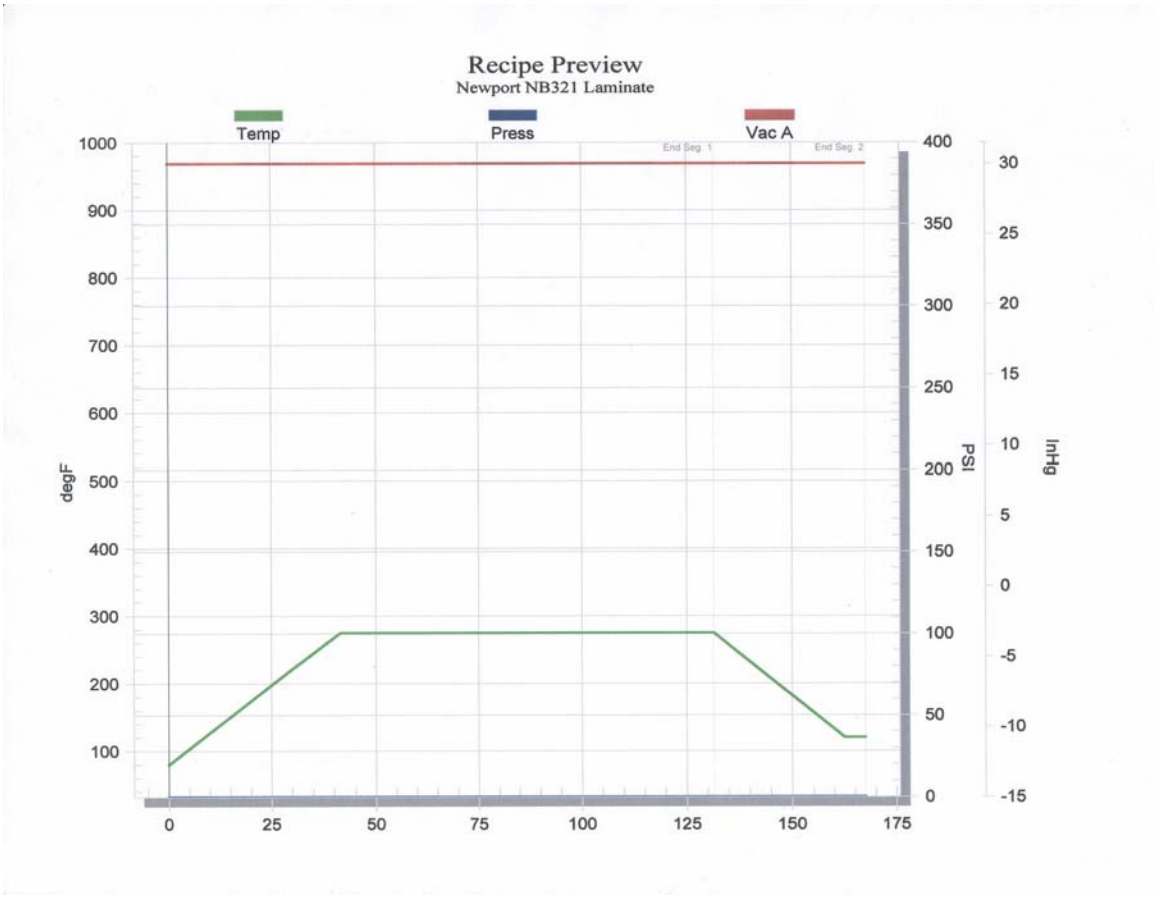


Figure 2.5b Cure cycle report for carbon adherend generated by auto clave.

The vacuum bagging procedure was carried out according to the standard practice in the industry. The stacking sequence varied slightly with optional layers and elements depending on the material being cured. Figure 2.6 depicts the vacuum bagging stacking sequence used in this investigation. Figure 2.7 shows a complete vacuum bag assembly with vacuum ports ready to be cured in the autoclave.

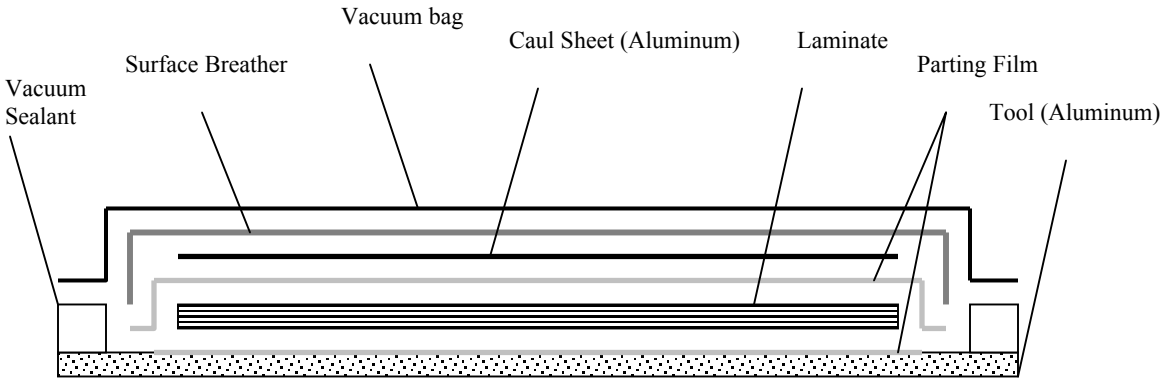


Figure 2.6 Vacuum bagging stack sequence.

Figure 2.7 Vacuum bag assembly.

### 2.2.2 Surface Preparation

Surface preparation of the panels to be bonded is an important step since it directly affects the strength of the adhesive bond that affects the failure mode. By preparing surface correctly, joint strength can be maintained to its full potential, resulting in long-term structural integrity. Incorrect surface preparation could lead to adhesive bond failure and unpredictable failure. The primary role of surface preparation is to remove surface contaminants, increase the bonding surface area, and improve surface roughness.

In this investigation, surface preparation was performed in accordance with the industry, adhering to the adhesive manufacturer recommendations. Surface roughness is a key factor in surface preparation. Sanding the surface to be bonded is the regular approach to increasing its roughness. However, hand sanding has a tendency to leave an uneven roughness across the panel surface. Sand blaster machines are often used because of their ability to sand a surface fairly even and the option to control pressure, thus allowing the user to achieve the required roughness intensity. Cured composite panels were trimmed to 18 inches by 18 inches to remove the extra resin deposited on the edges of the panels. Each panel was then cut in half with a table saw making two identical 9 inches by 18 inch panels as shown in Figure 2.8. The 9 inches by 18 inch panel pairs to be bonded together were then sand blasted using a pressure of 85 psi. A water break test was performed on all the panels to ensure the minimum roughness required for bonding. Panels were then left to dry in normal room conditions and cleaned thoroughly with acetone.

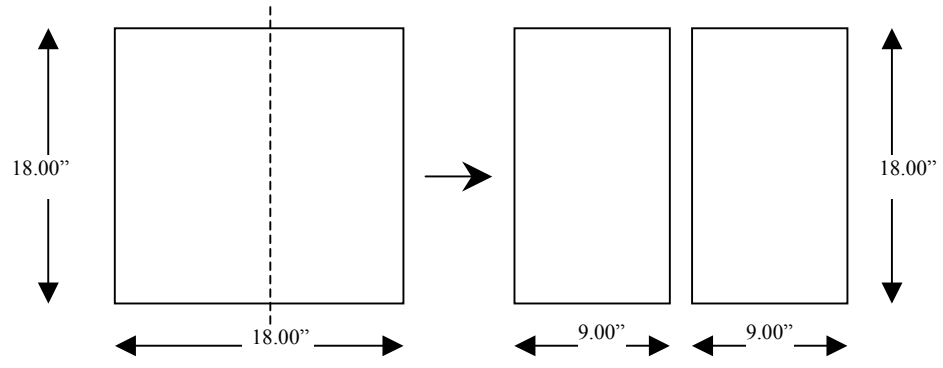


Figure 2.8 Panel resizing process.

### 2.2.3 Adhesive Selection and Bonding Method

Adhesive selection was based on the industry's use of adhesives on single-lap shear testing since it allows one to utilize the findings of this investigation to benefit the industry itself. Paste adhesive EA 9394 manufactured by Hysol is a widely used adhesive in the aviation industry, known for its proven high strengths in high-temperatures environments as well as low-temperature environments and long pot life, making it convenient to work with. Film adhesives have long being used in the industry for their convenience, less wastage, and high strength properties. The film adhesive EA 9628 manufactured by Hysol is a widely used film adhesive in the industry. Table 2.3 summarizes the features of both adhesives.

Table 2.3 Summary of features of selected adhesives.

| EA 9394 (Paste) | EA 9628 (Film) |
|---|---|
| Room Temperature Cure | Good Toughness |
| Good Gap Filling Capabilities | 235-250F/113-121C Cure |
| 350F/177C Performance | Bonds Many Materials |
| Potting Material | Excellent Durability |
| Room Temperature Storage | Film Adhesive |
| Long Pot Life | Less waste |
| Low Toxity | |

The above-mentioned adhesive types along with carbon and glass adherends introduced in the previous section were chosen to generate response curves. After narrowing down the adhesive and adherend types, the next step was to bond panels with proper care and cure then in appropriate temperature and pressure conditions. The two most important aspects of the bonding process are to maintain a constant bond-line thickness and a proper pre-crack simulation technique.

It was determined that a bond-line thickness of 0.015 inch was satisfactory to compare the results since the industrial adhesive joint bond-line thickness was within that range as were most thick single-lap shear coupons tested. Many techniques are being followed to maintain a constant bond-line thickness in test coupons. Glass micro-beads embedded in adhesives, metal spacers, and bladder pressure techniques are some of the popular techniques. Since the type of adhesives selected for this investigation do not contain micro beads, metal spacers were used to maintain the required bond-line thickness. After a few bonding trials, a spacer with a thickness of 0.01 inch was chosen for this investigation. Although the material of the spacers does not have an effect on the results, it should be noted that the spacers were made from brass. In order to make the panel bonding area uniform through-out, a bladder press was used because of its ability to control the pressure applied on the bonding panels.

After a number of trials using various methods to simulate an initial crack, it was determined that applying a few layers of utility tape to both sides of the initial crack area worked best. However, pre-cracking is important for specimens that are fabricated using this method in order to simulate a realistic cohesive crack. The number of utility tape layers should compliment the overall bond-line thickness of the specimen. Since the thickness of tape used was measured to be 0.0025 inch, it was determined that four layers of utility with two layers for each surface were necessary.

All the panels were bonded using the same technique in order to maintain the process consistency. Panels bonded with EA 9394 paste adhesive were cured at room temperature for five days, as recommended by the manufacturer, while EA 9628 film adhesive bonded panels were bonded in an oven at 250 $^{0}$F. All panels were bonded using the same bladder press with a constant pressure of 20 psi. Figures 2.9a though 2.9c show the panels bonded with spacers and adhesives, summarizing the bonding process mentioned above.

Figure 2.9a  Glass panels with spacers and utility tape.

Figure 2.9b  Glass panels with EA 9394 paste adhesive prior to bonding.

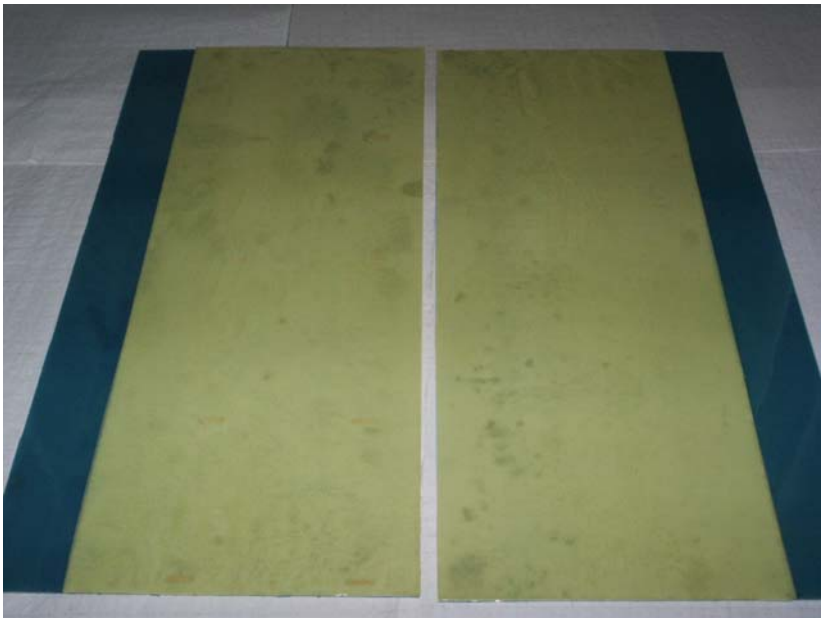

Figure 2.9c  Carbon panels with EA 9628 film adhesive prior to bonding.

**EA 9394 Paste Adhesive Bond Cure**

- Part A and part B mixed at a 100% to 17% ratio
- Five days at room temperature
- Pressure 20 psi

**EA 9628 Film Adhesive Bond Cure**

- Four layers of film
- One hour at 250 $^{0}$F
- Pressure 20 psi

## 2.3 Specimen Fabrication

This section explains the individual specimen fabrication process for test methods, mode I, mode II, and mixed-mode bending. It is important that each specimen shares the same dimensions and is free of contaminations, such as dust, extra adhesives and moisture. Fabrication process for mode I and mixed-mode specimens is identical. Mode II specimens require less work and are ready for testing once they are milled out of the bonded panels and the dimensions are measured. Five specimens were fabricated for each test method and for each adhesive-adherend combination.

Bonded panels were machined to the required specimen geometries using a milling machine. All test specimens fabricated to generate mixed-mode fracture toughness curves share the same geometry, thus making it convenient to mill the maximum number of specimens from the bonded panels. Although the basic specimen geometry is the same initial crack length varies between test methods as described in the background section of this chapter. This fact was taken into account when utility tape was applied to simulate the initial crack on each panel pair. Figure 2.10 is a schematic diagram of the milling process of the bonded panels avoiding spacers.

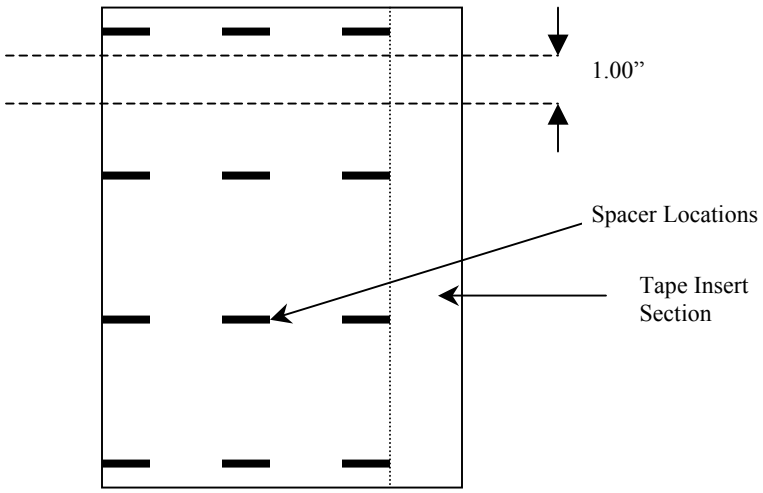


Figure 2.10 Schematic diagram of the milling process of the bonded panels.

Mode I and mixed-mode specimens require hinges at the opening to enable their attachment to the respective fixtures. Piano hinges were used for this purpose, and EA 9394 paste adhesive was chosen for its proven peel strength to bond the hinges to the specimen. Surface preparation for the hinge bonding was done by sanding both surfaces and cleaning them thoroughly with acetone. The curing process was the same as panel bonding with EA 9394 paste adhesive. Figures 2.11a and 2.11b are fabricated mode I and mode II specimens.

Figure 2.11a  Fabricated carbon mode I specimen.

Figure 2.11b  Fabricated glass mode II specimen.

All specimens were measured for geometric dimensions using a flat head caliper and bond-line thicknesses were measured using a microscope. All measuring apparatus were properly calibrated, and insert lengths were measured for each test method. Figure 2.12 is a diagram of the final specimen geometric dimensions. Table 2.4 summarizes the initial crack lengths of specimens for each test method.

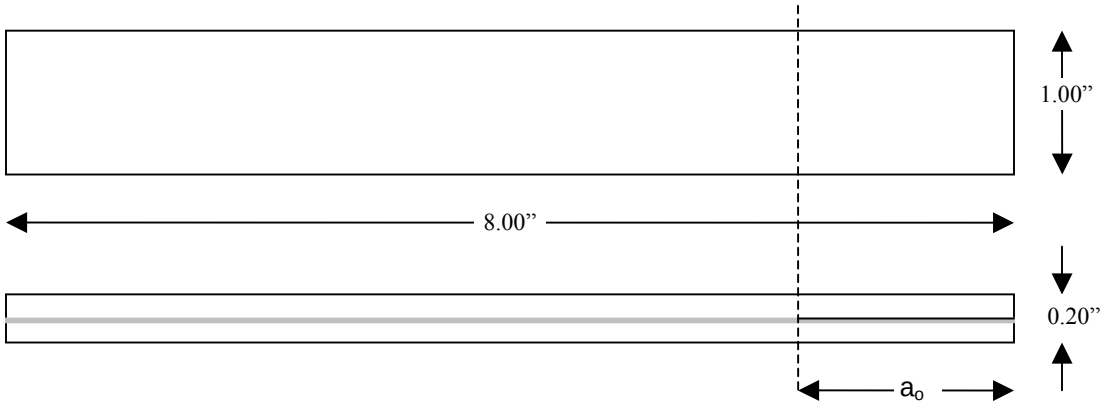


Figure 2.12 Geometric dimensions of specimens tested (top and side views).

Table 2.4 Initial crack lengths of specimens for each test method.

| Mode Mixity (%) | Standard ASTM, SACMA | Initial Crack, $a_o$ (in) |
|---|---|---|
| 0 – (Mode I) | D5528 | 2 |
| 5-95 (Mixed Mode) | D6671 | 1 |
| 100 (Mode II) | BMS 8-276F | 1.5 |

## 2.4 Data Point Generation

Data points required to generate the respective mode-mixity fracture toughness curves for the adhesive-adherend combinations described above were determined using three types of test methods. As discussed in the previous chapter, mode I and mixed-mode data points were generated in accordance with ASTM D5528 and D6671 standards, while mode II data points were generated using SACMA BMS 8-276F standard. The test matrix followed for the mixed-mode fracture toughness curve data point generation is shown in Table 2.5.

Table 2.4 Test matrix for mixed mode fracture toughness data generation

| Configuration | Mode I | Mixed Mode (%) | | | | Mode II |
|---|---|---|---|---|---|---|
| | | 25 | 50 | 70 | 80 | |
| Aluminum/9394 | 5 | 5 | 5 | 5 | 5 | 5 |
| Carbon/9394 | 5 | 5 | 5 | 5 | 5 | 5 |
| Glass/9394 | 5 | 5 | 5 | 5 | 5 | 5 |
| Carbon/9628 | 5 | 5 | 5 | 5 | 5 | 5 |
| Glass/9628 | 5 | 5 | 5 | 5 | 5 | 5 |

Testing was performed on a 5 kip servo hydraulic MTS machine with a 500 lb load cell. Each test method required a different fixture and an optimum test rate. Laminate properties required for the mixed mode bending ratio adjustment were determined using the Composite Laminate Analysis Systems (CLASS) software developed by Material Science Corporation. Individual laminar properties were obtained from the Advanced General Aviation Transport Experiments (AGATE) database maintained by the National Institute for Aviation Research [19].

### 2.4.1 Testing Procedure

**Mode I**

Mode I testing was conducted using a test fixture fabricated by Wyoming Test Fixtures in accordance with ASTM D5528. All specimens were tested at a rate of 0.05 mm/min on a 5 kip servo hydraulic machine with a load cell of 500 lbs. An optical microscope with a magnification power of 100x was used to locate the crack tip. MTS Basic TestWare was used for data acquisition. Load, displacement, and time were acquired from the test with an acquisition rate of 10 Hz. All specimens were precracked, as recommended by the ASTM standard [15]. Figure 2.13 shows the test setup used with a specimen.

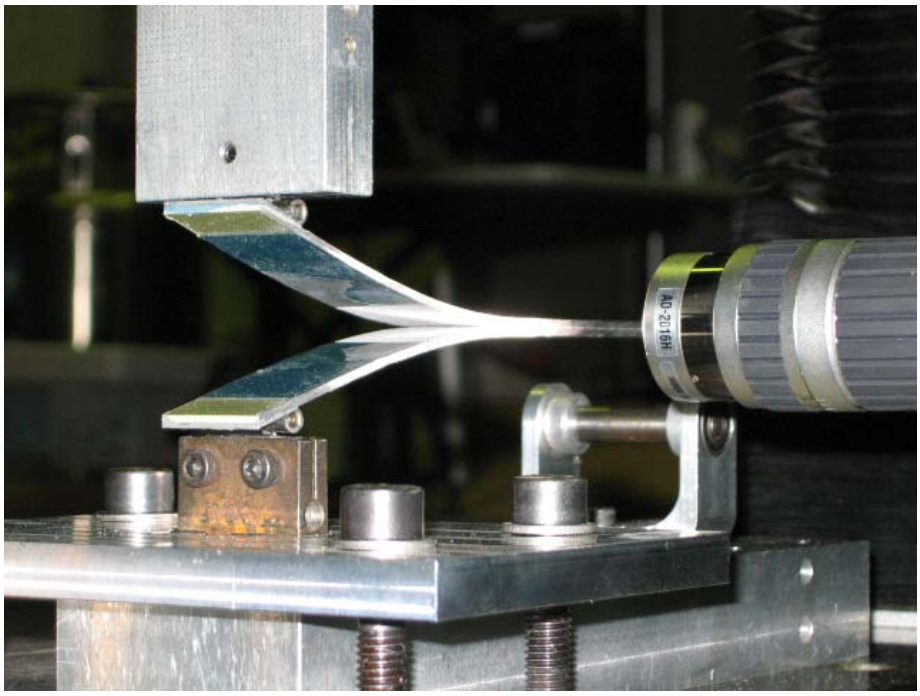

Figure 2.13 Mode I test setup with an aluminum specimen.

**Mode II**

Mode II testing was conducted using a three-point bend fixture fabricated by Wyoming Test Fixtures. All specimens were tested at a rate of 1 mm/min on a 5 kip servo hydraulic test machine with a 500 lb load cell. Specimens were precracked as recommended by the SACMA standard, and three propagation values were taken for each specimen. An optical microscope with a magnification power of 100x was used to locate the crack tip. The fixture was set up with a supporting span of 4 inches and a loading span of 2 inches. The initial crack length (insert) for precracking was 1.5 inch and the rest of the propagations were made with an initial crack length of 1 inch [16]. Figure 2.14 shows the test setup used for mode II testing.

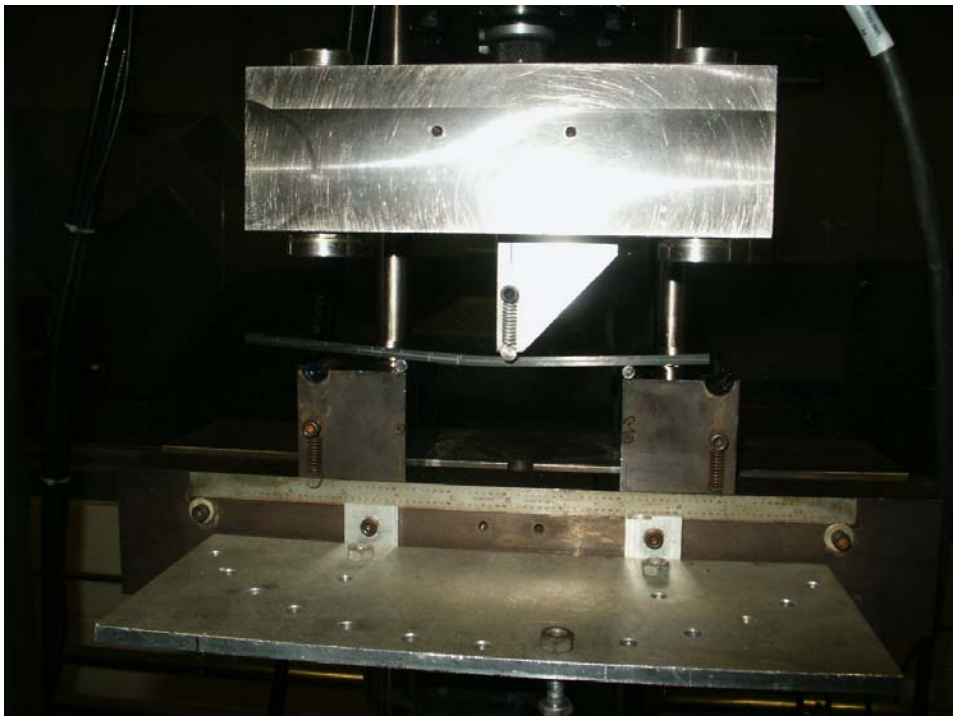

Figure 2.14 Mode II test setup with carbon specimen.

**Mixed-Mode**

Mixed-mode testing for the desired ratios was conducted using a mixed-mode bending fixture fabricated by Wyoming Test Fixtures in accordance with ASTM D6671 on a 5 kip servo hydraulic test machine with a 500 lb load cell. Figure 2.15 depicts the test setup used in this investigation with an optical microscope with a magnification power of 100x to locate the crack tip. The data acquisition procedure was the same as for mode I and mode II tests. The lever length was adjusted to obtain the desired mix ratio in accordance with the standard using the laminate properties of each adherend. It was determined to use one lever length for each mode-mixity ratio on all specimens since the calculated lever lengths only varied one $100^{th}$ of an inch. Table 2.5 shows the lever lengths used for each mode mixity.

Table 2.5 Lever lengths used for mode mixity ratios.

| Mixity (%) | 25 | 50 | 70 | 80 |
|---|---|---|---|---|
| c (in) | 3 | 1.7 | 1.25 | 1.1 |

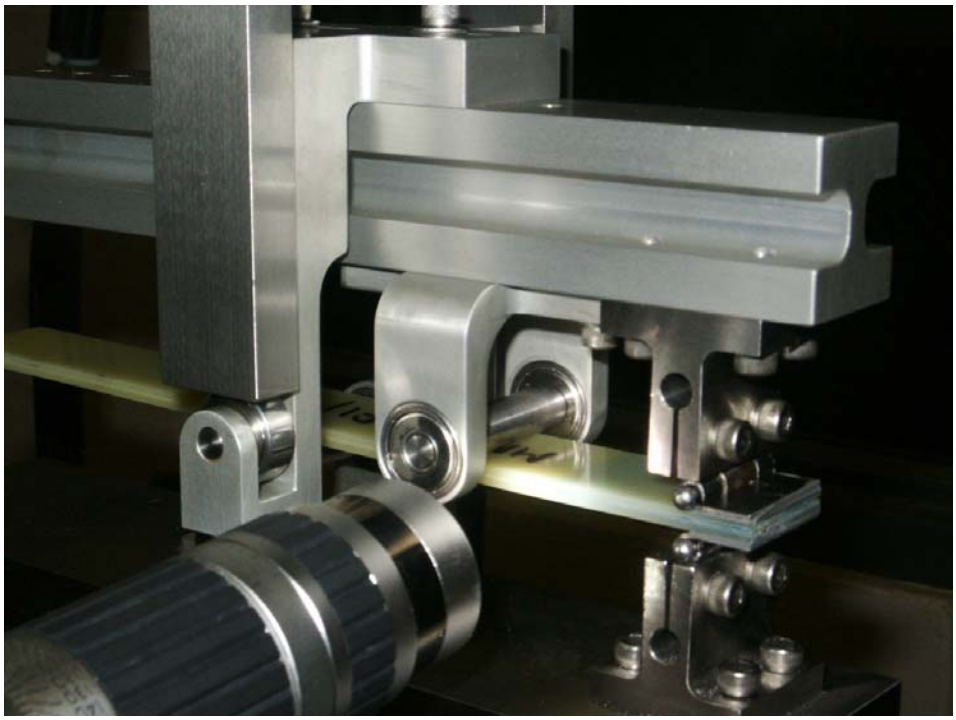

Figure 2.15 Mixed-mode test setup with a glass specimen.

In order to make the mixed-mode fracture toughness curve valid for the adhesives used, it is important to make a cohesive failure. Only the cohesively propagated or initiated specimens were used in data analysis. Figures 2.16a and 2.16b show typical initial failure modes for the two adhesive types.

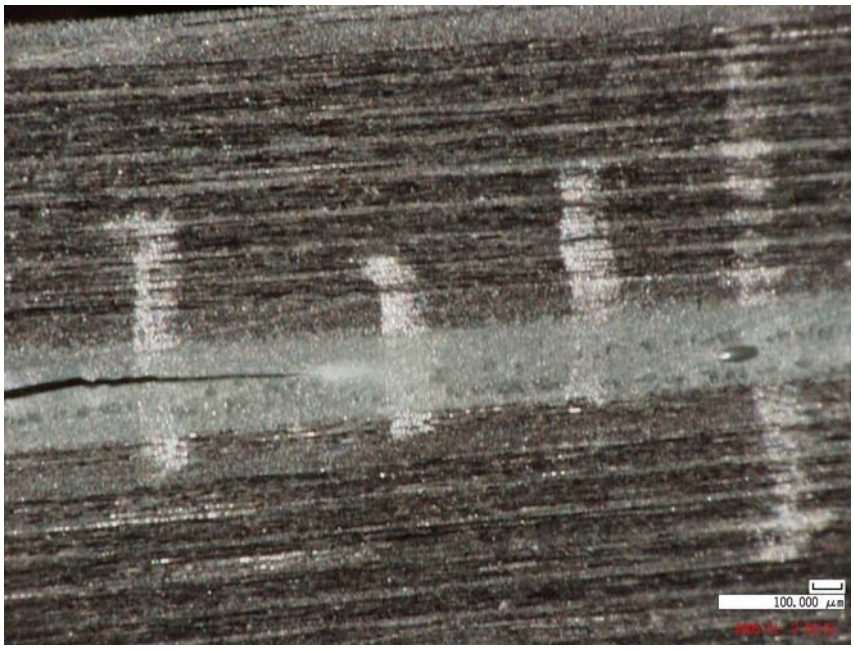


Figure 2.16a  Cohesive failure of a carbon/9394 specimen.

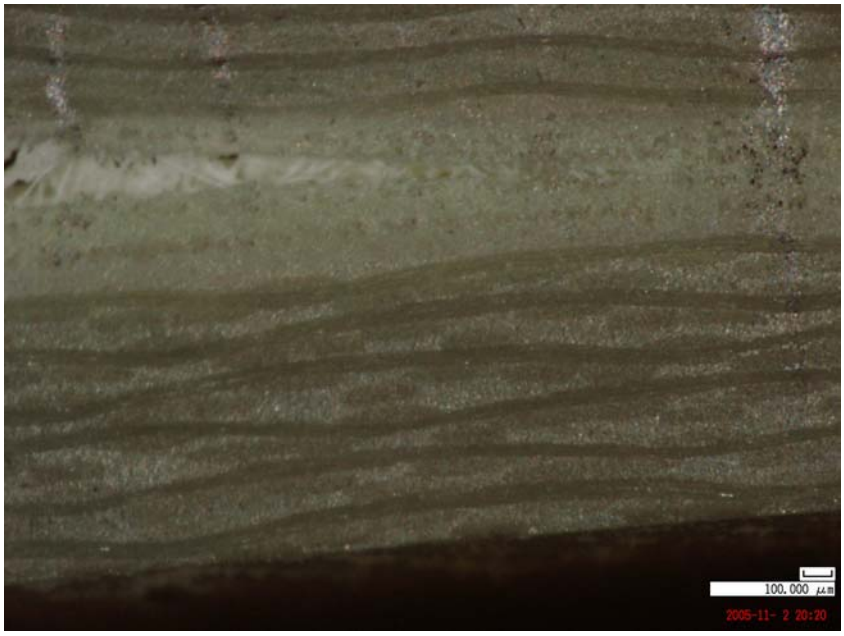


Figure 2.16b  Cohesive failure of a glass/9628 specimen.

### 2.4.2 Data Reduction

Data obtained from the data acquisition apparatus were then further processed according to each standard to generate strain energy release rate values. It is important to stress that only the crack initiation point was considered in this investigation. Typically each test method recommends obtaining three critical strain energy release rate values corresponding to initiation.

- $G_C$ (NL) - corresponds to the point where load Vs displacement curve of the test becomes non-linear.
- $G_C$ (5%/max) - corresponds to the point where a line 5% offset of the slope intersects the load displacement curve or the maximum load point, whichever occurs first.
- $G_C$ (VIS) - corresponds to the point where the actual crack initiation is visually observed by the testing personnel.

The critical strain energy release rate that was visually observed, $G_C$ (VIS), was used in this investigation due to the fact that the nonlinear point is too conservative and may be the best approach for design purposes, and the maximum point may overlook the actual propagation of the crack tip. However, in some cases where unstable crack propagation was observed, all three points were assumed to be the same data point.

An SI unit system was adopted during the data reduction segment of this investigation since critical strain energy release rates are stated in $kJ/m^2$ (SI units) in the literature, hence, allowing one to conveniently compare results. Formulas used in calculating the values are discussed in the early part of this chapter in equations 2.2 to 2.5. Typical load displacement curves are shown in Figures 2.17a and 2.17b. Strain energy release rate values generated experimentally for all specimen types are shown in Appendix A.

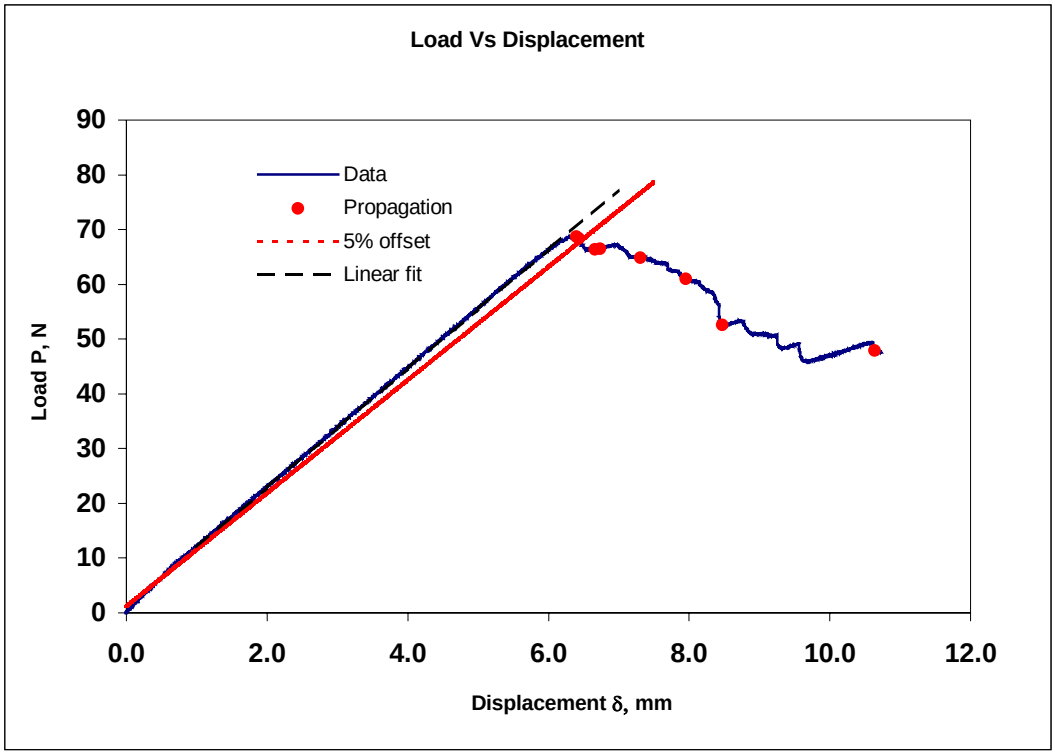


Figure 2.17a Typical load displacement graph after data reduction in mode I and mixed mode.

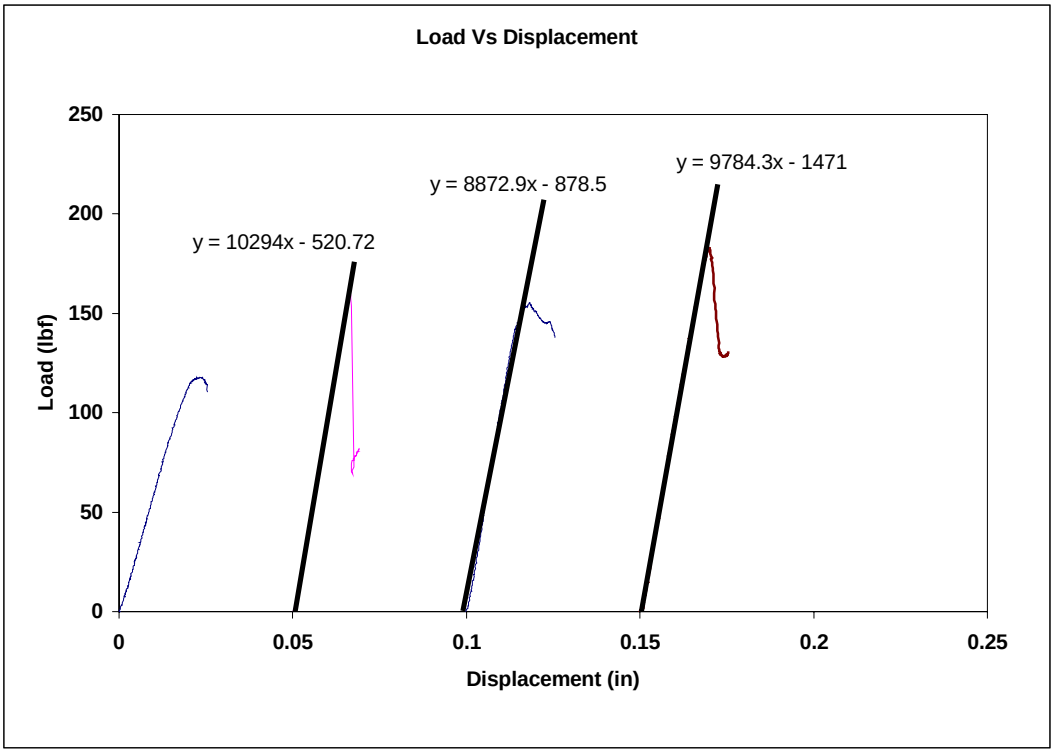


Figure 2.17b Typical load-displacement graph after data reduction in mode II.

# CHAPTER 3

# SINGLE-LAP JOINT TESTING

The single-lap joint test method recommended by ASTM D3165 is intended to determine the shear strength of adhesively bonded joints. Although this test method is designed for metal adherend joints, the standard document states that it may also be used with other adherends such as composites [3]. Industry has been using this method successfully to determine shear properties of adhesively bonded composite joints. In this investigation, single-lap joint data is used to confirm the methodology developed to predict the failure load or stress of a given adhesive joint. The test specimen configuration recommended by ASTM 3165 involves some machining issues especially with composite adherends that affect the overall test results; hence, it was determined to use a slightly different configuration to eliminate the imperfections of the simulated adhesive joint.

Adherend and adhesive selection was the same as discussed in previous chapters since the mode-mixity fracture toughness curves generated were intended as a tool to predict the failure load of the single-lap joint. It is important to maintain the same bond-line thickness and other physical characteristic in the single-lap shear specimens as the specimens tested for fracture toughness in the previous chapter in order to minimize the dependent variables. Bonding procedures were the same as those used on previous specimens since the adhesive and adherend types were the same.

The test method and apparatus used for single-lap shear strength determinations were the same as the ASTM standard recommendations including data reduction procedures. Failure modes of the test specimens were closely examined to ensure the similarities to the fracture toughness specimen failure modes.

## 3.1 Background

The specimen configuration recommended by ASTM 3165 often involves a major manufacturing issue when it comes to using composite adherends. The two notches in the two bonded adherends ideally should be through the adhesive layer and just touching the adjacent adherend. However, machining precisely to meet this requirement is difficult due to the errors in milling blades and the un-uniformity of the adherend and adhesive thickness. Specimens machined this way often have a thin layer of adhesive left or a thin layer of adherend cut away, thus reducing the adherend strength since it is a composite laminate. Figure 3.1 shows this effect on the recommended specimen configuration. Taking this issue into account, a slightly modified specimen configuration was used in this investigation, as shown in Figure 3.2.

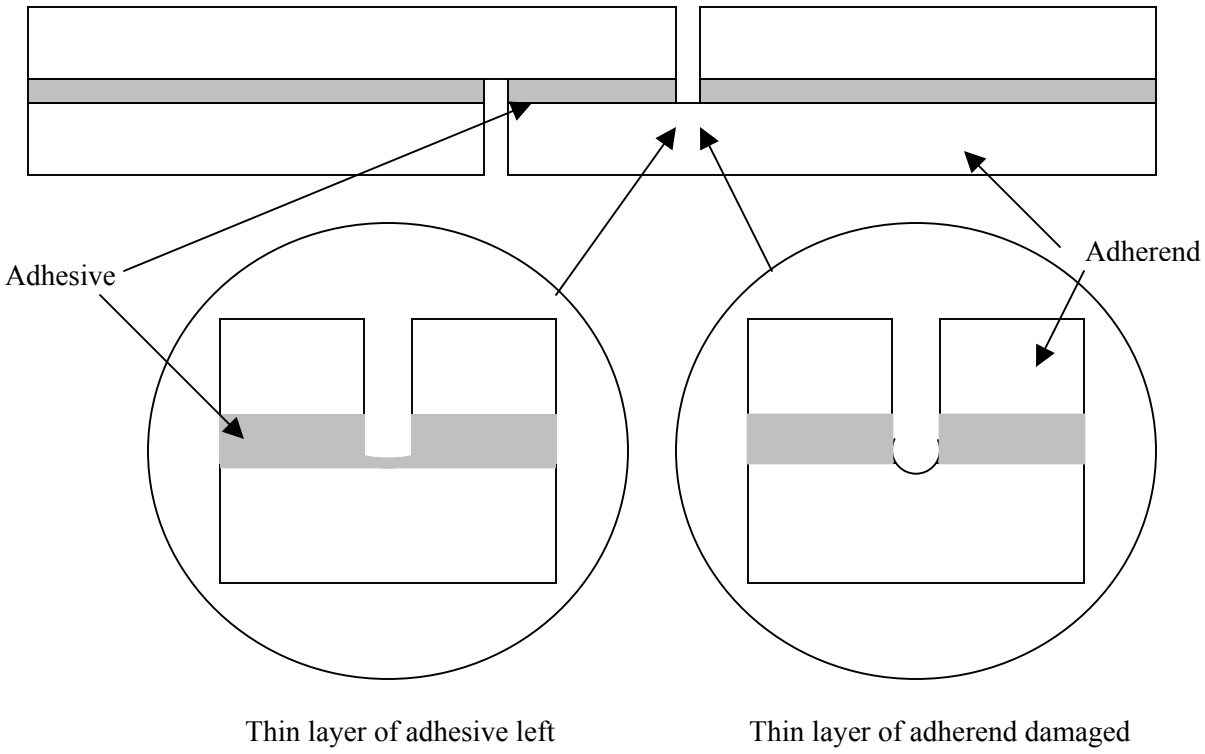


Figure 3.1 Milling issues of ASTM 3165 recommended specimen configuration.

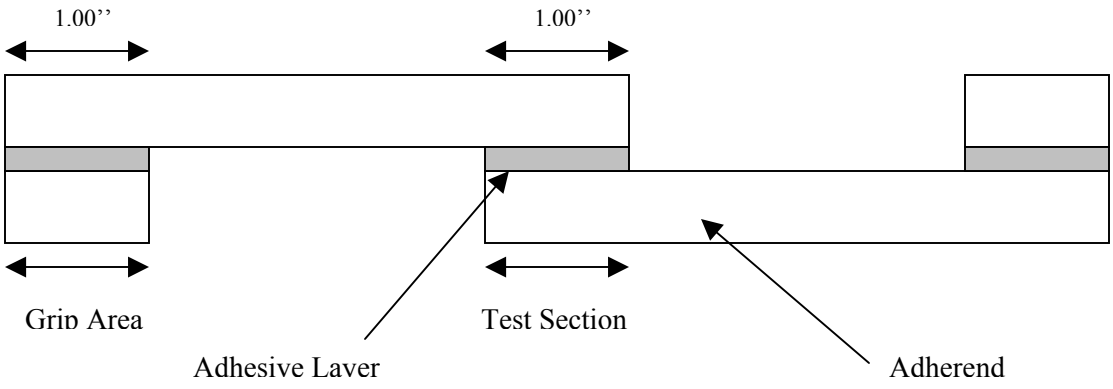


Figure 3.2 Specimen configuration used in this investigation.

The exact specimen dimensions depend on the adherend and adhesive type used in the bonded joint. Specimens used in this investigation share the same bond-line and adherend thickness as the fracture toughness specimens previously discussed, since the same panels and adhesive types were used.

ASTM standards recommend applying a tensile load along the length of the specimen in displacement control at a constant speed of 0.05 in/min until the specimen fails at the test section. Shear strength of the bonded joint was calculated using equation 3.1.

$$\tau = \frac{P}{wl} \tag{3.1}$$

where,

$P$ = Load at failure, lbs
$w$ = Width, in
$l$ = Test section length, in
$\tau$ = Shear strength, psi

## 3.2 Specimen Fabrication

The specimen fabrication process for single-lap shear was approached similarly as fracture toughness specimen fabrication discussed in chapter 2. The same panels along with the same adhesive types and cure cycles were used in the bonding process. The specimen configuration introduced in the previous section allows for bonding the adherend and grip sections separately, thus reducing the machining time and eliminating the imperfections discussed above. The bond-line thickness was maintained using the same brass spacers along the bonded region.

The first step in specimen fabrication was to resize the original panels into adherend sections and grip sections according to the final expected specimen geometric dimensions. Surface preparation of the bonding areas of the adherend sections and grip sections were done similarly, using a sandblaster. Utility tape was used to serve a different purpose in this fabrication process compared to that for fracture toughness specimens. Utility tape was applied to the outside of the bonding region to remove the excess adhesive when curing under pressure. Figures 3.3a and 3.3b summarize these steps for a glass adherend bonding process.

Panels were bonded using a bladder press with a pressure of 10 psi following the same cure cycle process in section 2.2.3. Paste adhesive EA 9394 was cured at room temperature for five days and film adhesive EA 9628 was cured at 250 $^{0}$F for one hour. Individual specimens were then milled, avoiding the spacer location, as shown in Figure 3.4.

Individual specimens were ready for testing once the geometric dimensions and bond-line thickness were measured. Geometric dimensions were measured using a flat head caliper, and bond-line thicknesses were measured using a microscope. All the apparatuses were properly calibrated according to manufacturer standards. Figure 3.5 shows a single-lap shear specimen ready for testing.

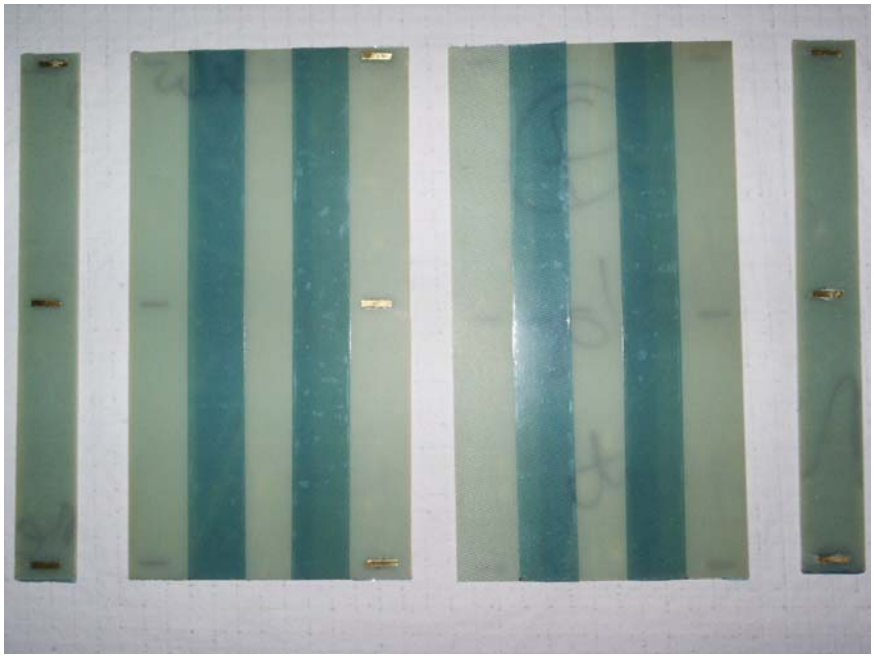

Figure 3.3a  Glass single-lap shear specimen fabrication process prior to bonding.

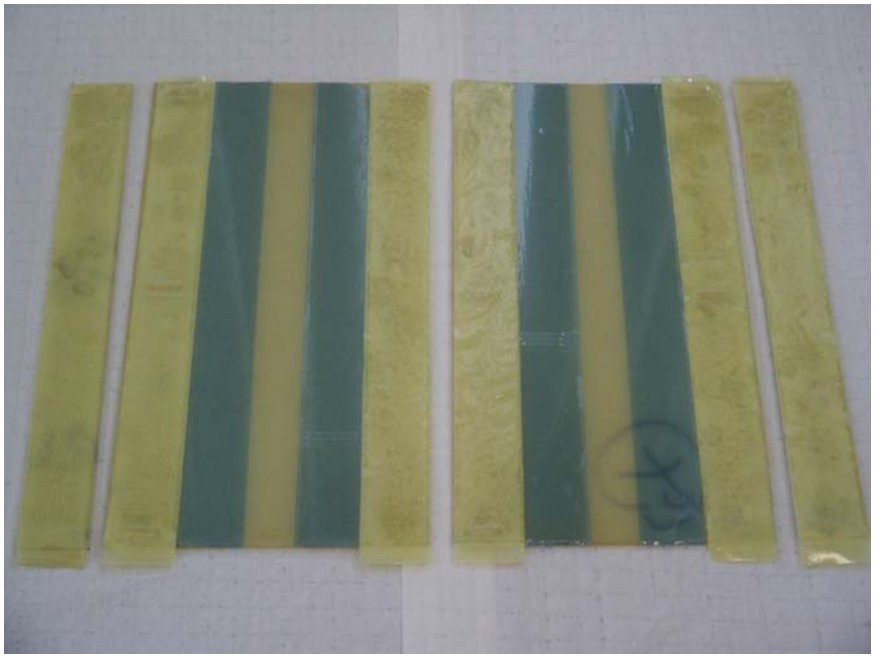

Figure 3.3b  Glass single-lap shear specimen fabrication process with film adhesive.

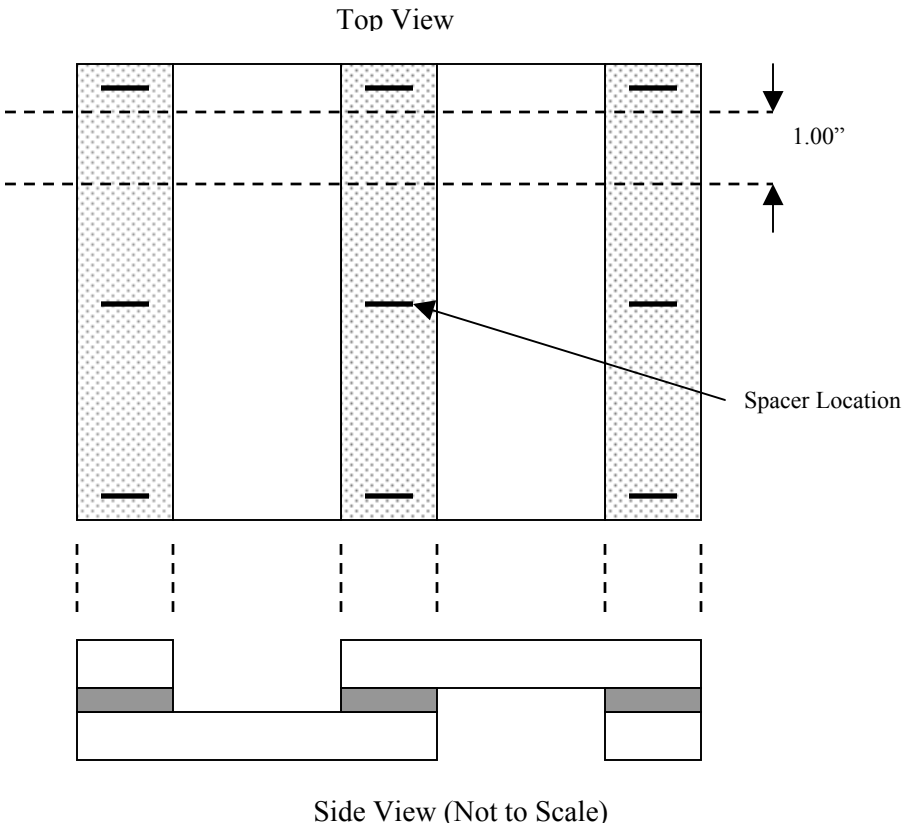


Figure 3.4 Schematic diagram of the milling process for individual specimens.


Figure 3.5 Carbon/EA9394 single-lap shear specimen.

## 3.3 Testing

Single-lap shear testing was conducted in accordance with the ASTM D3165 standard using a 22 kip servo hydraulic with a test rate of 0.05 in/min in displacement control. Hydraulic clamping grips were used to attach the specimen to the test frame. Attention was given to proper alignment in order to avoid bending and asymmetric loading. After some trial specimens, grip pressure was set to 1000 psi. It is important to clamp the specimens in load control allowing minimum stress in the adhesive gage section of the specimen. Load and actuator displacement data was collected using TestWorks software with a data acquisition rate of 10 Hz for all specimens. Figure 3.6 is the test setup used for a carbon/9394 specimen.

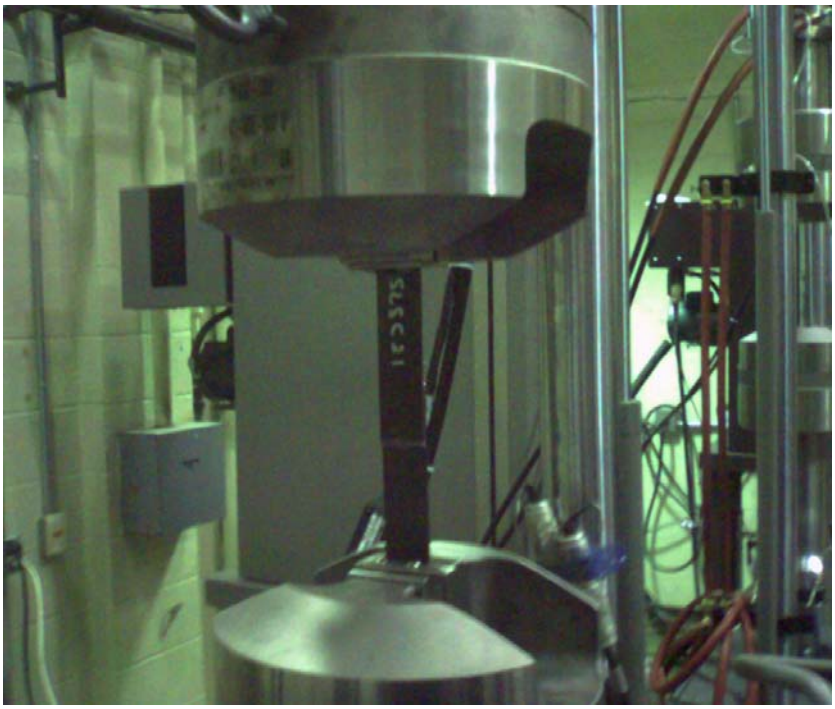

Figure 3.6 Single-lap shear test setup.

Most single-lap shear specimens with composite cross ply laminates usually fall into the adherend failure criteria. In this investigation, the initiation of the failure was observed to be cohesive on all specimens since a thin strip of adhesive was seen on both faces of the test section adherends, as shown in Figures 3.7a and 3.7b. Appendix A. shows the apparent shear strengths obtained experimentally for all the specimen types.

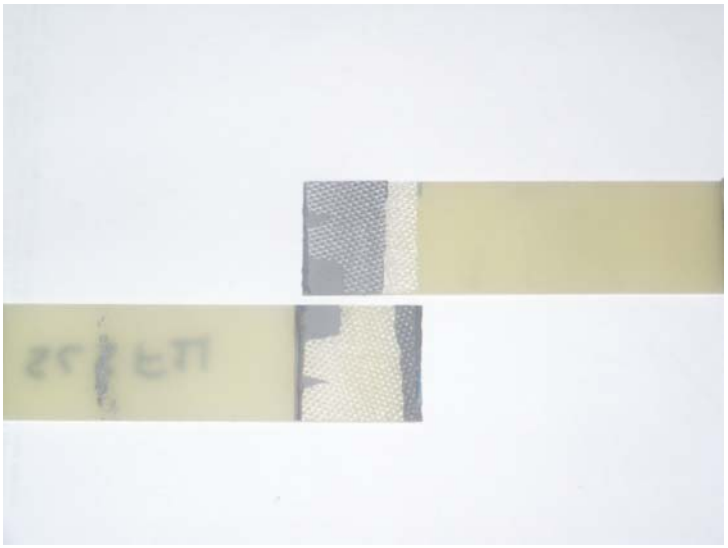

Figure 3.7a  Failure modes of glass/9394-cohesive failure at initiation.

Figure 3.7b  Failure modes of carbon/9628-cohesive failure at initiation.

# CHAPTER 4

# FINITE ELEMENT MODELING AND ANALYSIS

Finite element method (FEM) analysis is a crucial part of this investigation since it serves as a tool in developing the failure load prediction method. FEM is a proven analytical tool used in the industry mainly to simulate stresses and strains of any structural part given the material properties and loading configuration. Complexity of the finite element method increases with the part's geometry as well as material behavior and meshing technique, since the core of this method relies on dividing the given part into elements and solving at an elemental scale. Hence, finer the mesh, the more accurate the results are.

Commercial finite element (FE) codes are readily available to simulate almost any kind of a structural component. Reliability, cost, and user-friendliness drive the preference of one code over another. Analytical models using low cost commercial solvers such as MAPLE, MATHEMATICA, etc. are an alternate approach. The laminated plate theory based analytical model developed by Huang H. et al. [17] to determine stress and strain distributions of a single-lap adhesive-bonded composite joint under tension is such an approach. This investigation required a tool that could determine the strain energy release rate of a cohesive crack, a step beyond the stress and strain analysis. Fracture Analysis Code 2D (FRANC2D) is a finite element based software package developed by Cornel Fracture Group that is freely available over the World Wide Web. FRANC2D has been successfully used as a fracture analysis tool to determine stress intensity and proved to be reliable [18]. This package was used to model single-lap joint specimens tested with different adherend-adhesive combinations, as discussed in the previous chapter. Laminate properties were calculated using the CLASS software introduced in Chapter 2 with laminar properties published in the AGATE database [19]. Manufacturer-published adhesive properties were used for both adhesive types.

## 4.1 FRANC2D Modeling

The FRANC2D software package includes the modeling tool CASCA, which allows the user to design the desired model to the appropriate proportions. It should be noted that this software package does not allow switching from one unit system to the other. Hence, units should be consistent throughout the entire process. Single-lap shear specimens were modeled using the English system, with the average geometric dimensions measured on the specimens fabricated in Chapter 3 and shown in the Figure 4.1. CASCA also requires the model to be meshed with the appropriate element type.

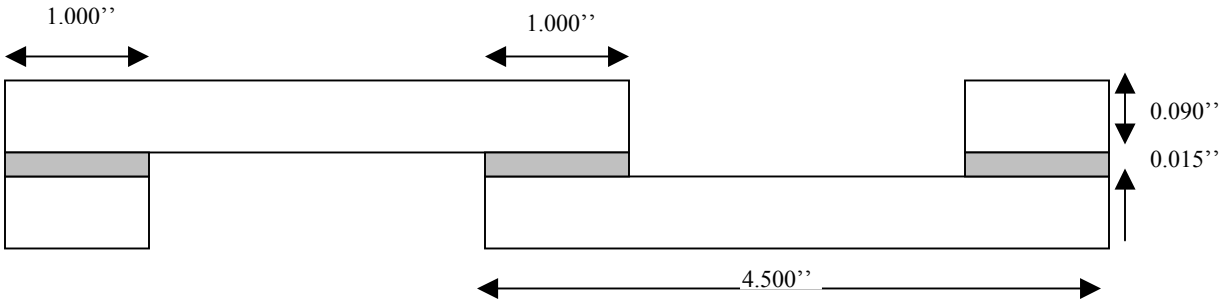


Figure 4.1 Schematic diagram of the single-lap specimen with dimensions used for modeling.

Two-dimensional eight noded (Q8) quadratic elements with bilinear 4side option were used throughout the entire specimen mesh. In order to simulate adherend and adhesive layers separately, it was necessary to model material regions allowing the user to assign material of choice. Although material properties are located in FRANC2D preprocessor sections, CASCA allows one to model different closed regions on a part. The input file generated from CASCA is then opened in FRANC2D and followed through the preprocessor steps to assign material properties, constrains, loads, etc. Figure 4.2 is a meshed model of the single-lap joint specimen on CASCA (showing only the gage section).

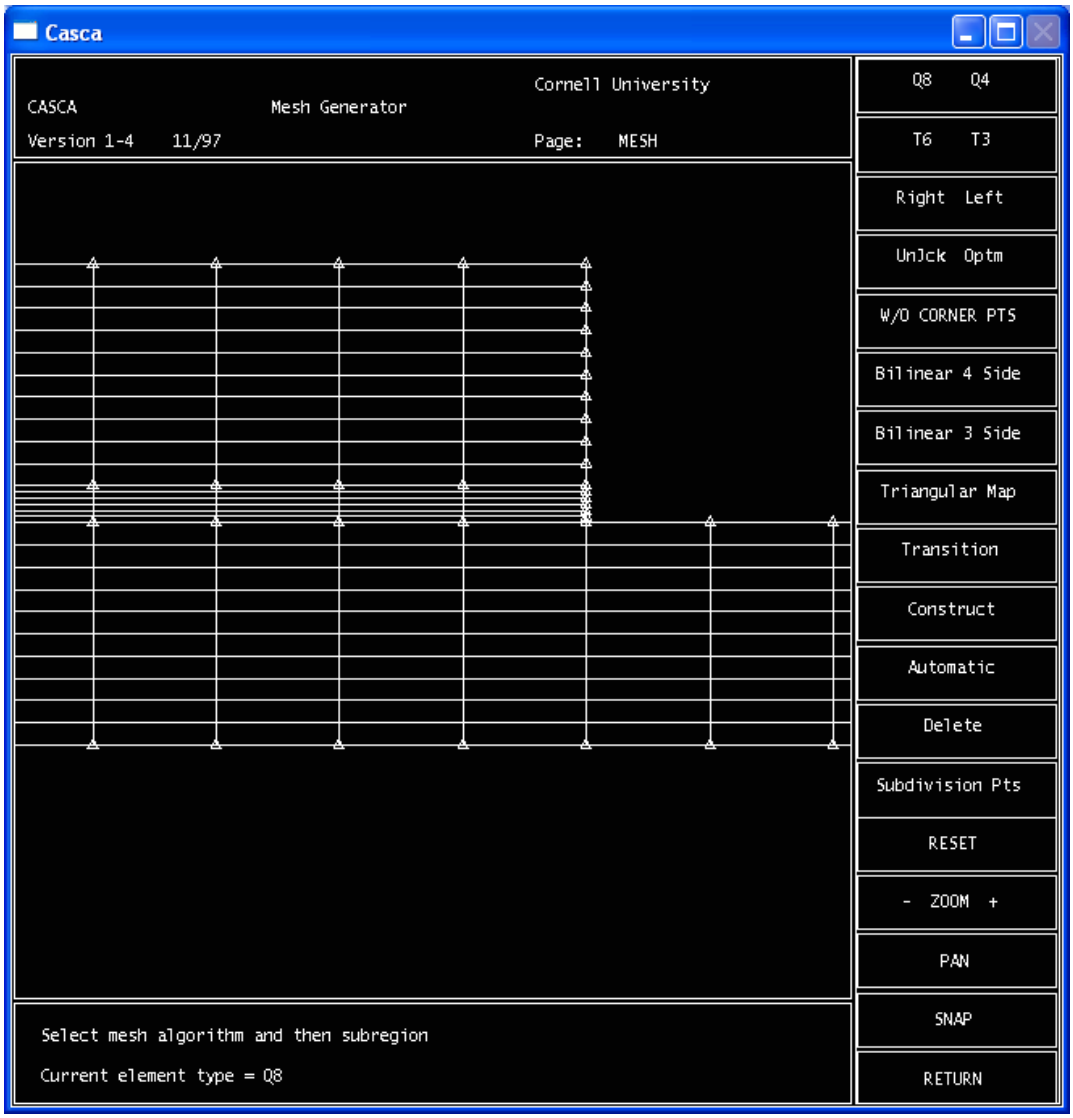


Figure 4.2 Meshed single-lap shear model on CASCA (gage section).

Loading the specimen in tension along the x-direction is simulated by applying pressure at one end of the specimen along the height while fixing the opposite end of the specimen in all directions. FRANC2D permits six load cases. Taking the failure loads of the tested specimens into account, appropriate loads were applied by varying the pressure. The next step was to apply a small crack to simulate the initiation of the failure of the specimen.

FRANC2D has the option to insert a crack at a desired location and define the crack tip location and the elements. Once the crack tip is defined, the code automatically defines a plastic zone and the elements around the crack appropriately. Quadratic 6 noded triangular (T6) elements were used to model the area around the crack. Additional elements may be added at the user's discretion. Figure 4.3 illustrates the crack simulations on FRANC2D. Numbers indicate the material type of the elements in the adherend and adhesive regions.

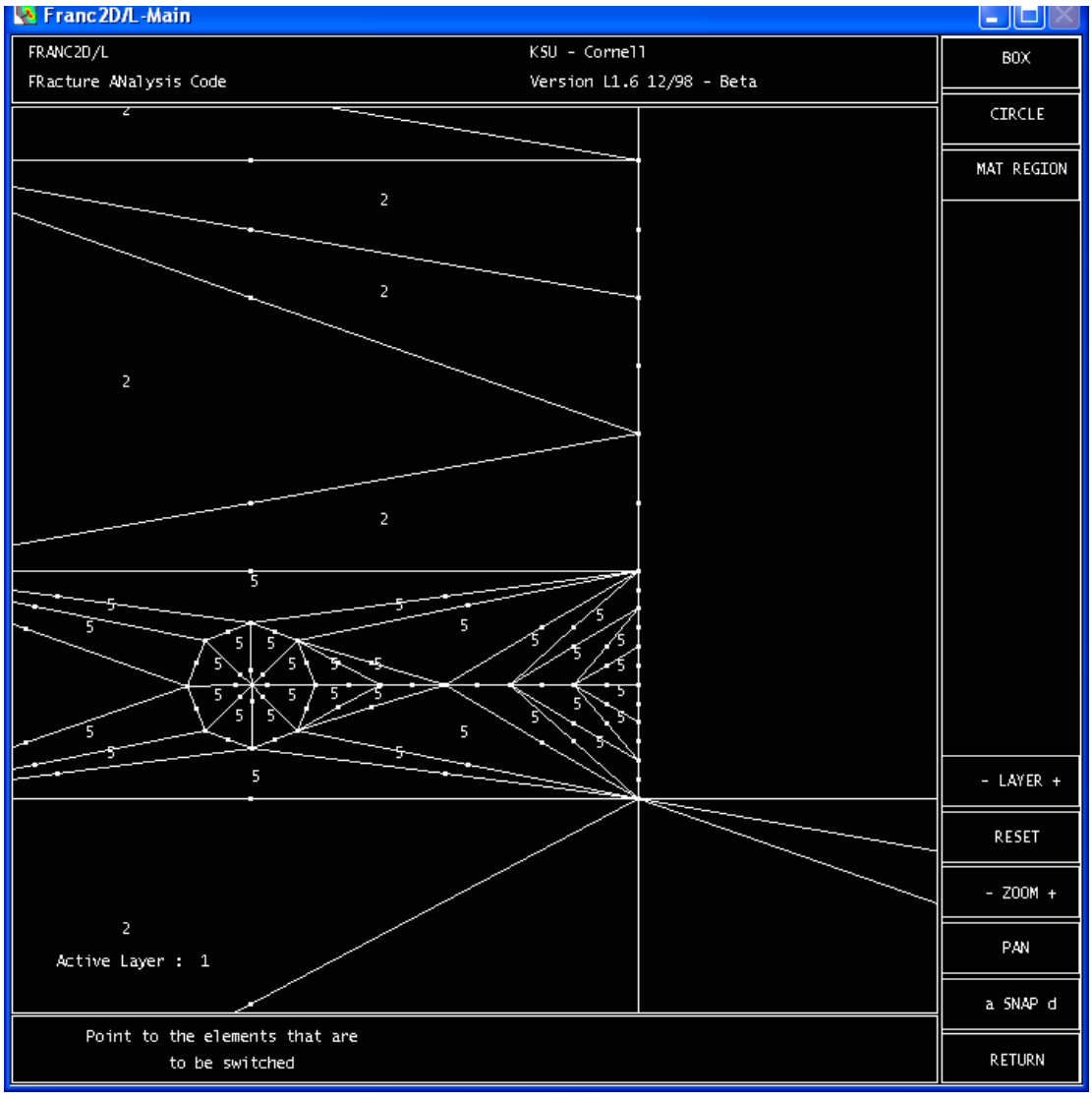


Figure 4.3 Cohesive crack simulations in the gage section on FRANC2D.

## 4.2 ASSUMPTIONS

This investigation was limited to linear elastic behavior, hence, all the equations used to obtain fracture toughness values from experimental methods discussed in previous chapters reflect linear elasticity. It should be noted that by making the same assumptions, FRANC2D simulation of the single-lap joint specimens may affect the results to a certain degree. Below is a list of assumptions made in the modeling and analysis segments of FEM analysis.

- Adherend laminates were modeled with elastic orthotropic material.
- Adhesive region was modeled with elastic isotropic material.
- Elastic behavior was assumed throughout the entire analysis.
- Cohesive failure initiation was assumed.
- Average dimensions of the specimens tested were used for the model.

## 4.3 FRANC2D Analysis

The Analysis segment of the code provides several options to calculate the strain energy release rate. Modified crack closure technique and J-integral are two popular options. Since the adhesive and adherends were assumed to behave only in the elastic region, J integral was used to determine strain energy release rates at the crack tip.

**J Integral**

J integral is a path-independent contour energy integral formulated by Rice and used for evaluating fracture toughness of elastic-plastic material [5]. J integral is approximately the same as the strain energy release rate, G, in the elastic region. Components of the J integral in mode I and mode II directions are $J_I$ and $J_{II}$, similar to $G_I$ and $G_{II}$. Formulation of the J integral is summarized in Figure 4.4, with the simplified components assuming small strains.

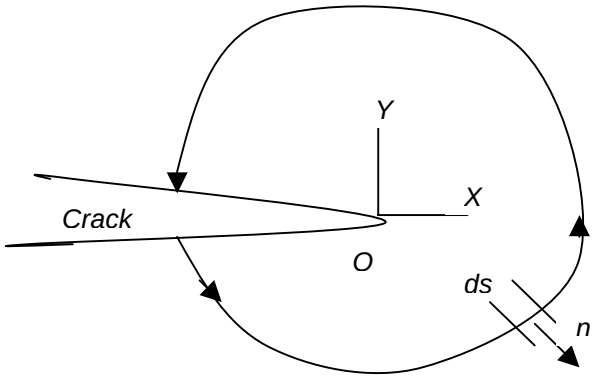


$$J_I = \frac{1}{2} h(\tau_{22}\varepsilon_{22})$$

$$J_{II} = \frac{1}{2} h(\tau_{12}\varepsilon_{12})$$

$$J = \oint_\Gamma w dy - T_i \frac{\partial u_i}{\partial x} ds$$

where; $w = \int_0^{\varepsilon_{ij}} \sigma_{ij} d\varepsilon_{ij}$ is the strain energy density, $T_i = \sigma_{ij} n_j$ is the traction vector, and h is the adhesive thickness

Figure 4.4 Formulation of J integral.

FRANC2D simulations of the stress fields are shown in the post-processor section as illustrated in Figure 4.5.

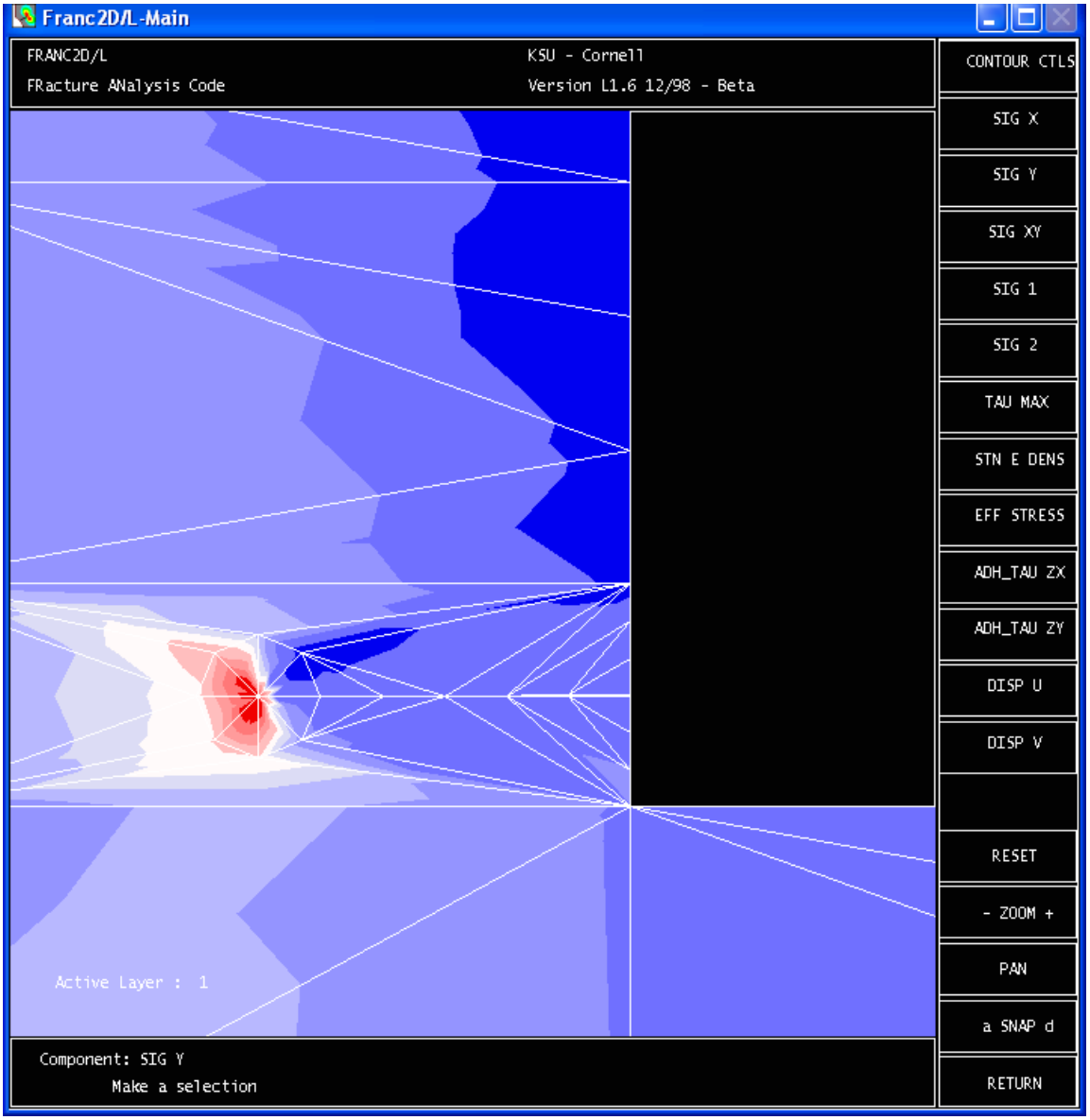


Figure 4.5 Stress field simulation of the section with the crack.

# CHAPTER 5

# RESULTS AND DISCUSSION

This chapter presents the results obtained experimentally from mixed-mode fracture toughness testing and single-lap joint testing. Numerically calculated results using FRANC2D are also presented. The proposed methodology to predict failure of a bonded joint is illustrated using a single-lap joint configuration. Adherend effects on mixed-mode fracture toughness results and the proposed failure prediction method are discussed. In addition the proposed methodology to predict the failure initiation of an adhesive joint using mixed-mode fracture data is outlined.

## 5.1 Experimental and Finite Element Result

Mixed-mode fracture toughness curves were generated using the data obtained from mixed-mode fracture toughness testing. Curves were plotted for the two types of adhesives, EA 9394 and EA 9628. Three types of adherends were used with EA 9394 in mixed-mode testing resulting in three curves. Two types of adherends were used with EA 9628 thus generating two curves. Single-lap joint specimens were tested for the two adhesive types as illustrated in Chapter 3. Failure loads obtained were used to determine apparent shear strengths.

Mode-mixity values for the single-lap joint specimens tested were obtained from FRANC2D. Furthermore, applied load and corresponding strain energy release rates were calculated for each adhesive-adherend combination single-lap joint specimen using FRANC2D. Load vs. strain energy release rate values were plotted to obtain the relationship between the applied load and the strain energy release rate at the joint assuming a small crack.

### 5.1.1 Mode-Mixity Fracture Toughness Curves

Tables 5.1a and 5.1b presents mixed-mode fracture toughness values obtained and Figures 5.1a and 5.1b presents the mixed-mode fracture toughness curves generated for the two adhesive types.

**Hysol EA-9394 Pate Adhesive**

Table 5.1a Critical strain energy release rate values for EA 9394 paste adhesive.

| Mode Mixity (%) | $G_C$ (VIS) (kJ/m2) | | |
|---|---|---|---|
| | Aluminum/9394 | Carbon/9394 | Glass/9394 |
| 0 | 0.422 | 0.352 | 0.425 |
| 25 | 0.615 | 0.411 | 0.378 |
| 50 | 0.652 | 0.600 | 0.657 |
| 70 | N/A | 0.679 | 0.698 |
| 80 | 0.788 | 0.704 | 0.634 |
| 100 | 1.279 | 0.924 | 0.901 |

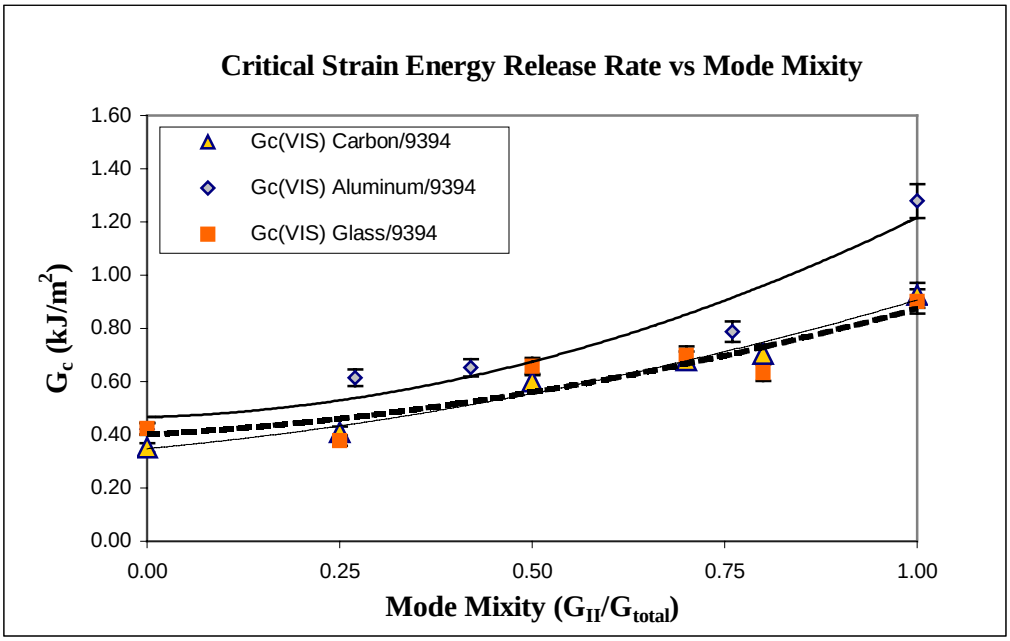


Figure 5.1a Mode mixity-fracture toughness curve for EA9394 paste adhesive.

**Hysol EA-9628 Film Adhesive**

Table 5.1b Critical strain energy release rate values for EA 9628 film adhesive.

| Mode Mixity (%) | $G_C$ (VIS) (kJ/m2) | |
|---|---|---|
| | Carbon/9628 | Glass/9628 |
| 0 | 0.350 | 0.350 |
| 25 | 0.411 | 0.500 |
| 50 | 0.539 | 0.605 |
| 70 | N/A | 0.674 |
| 80 | 0.805 | N/A |
| 100 | 0.857 | 0.824 |

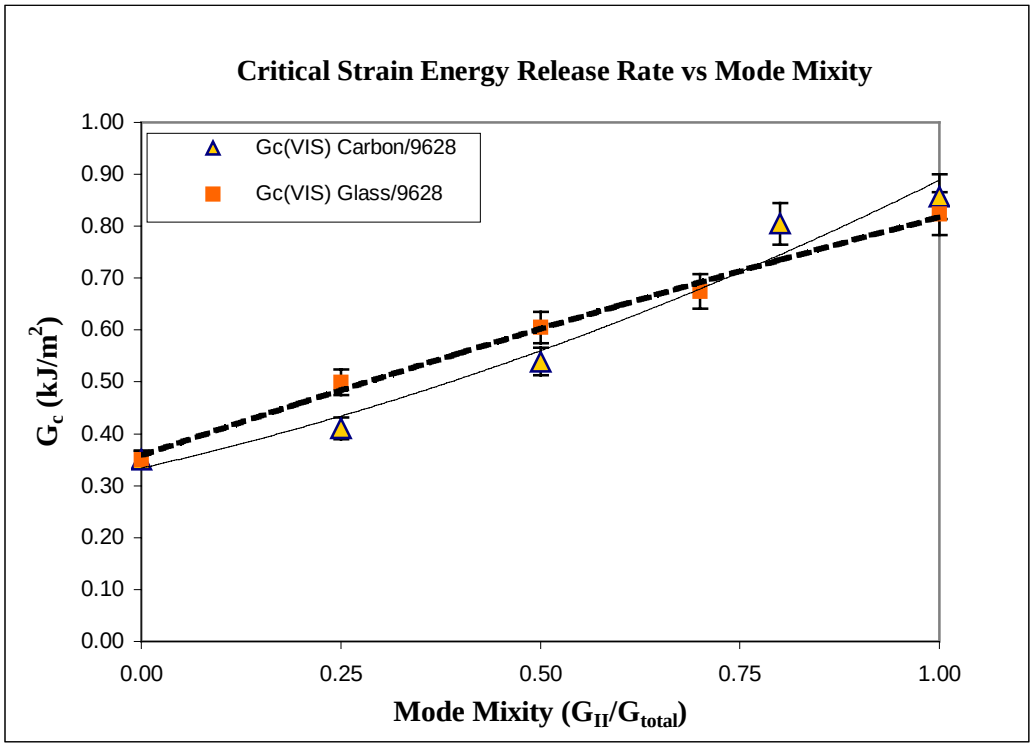


Figure 5.1b Mode mixity-fracture toughness curve for EA9628 film adhesive.

### 5.1.2 Single-lap joint specimen data

Failure loads obtained from testing single-lap joint specimens for the two adhesive-adherend combinations were then divided by the individual specimen overlap area to determine the apparent shear strengths. Table 5.2 provides a summary of the average values.

Table 5.2 Summary of shear stress at failure for all specimen combinations.

| Adhesive | Adherend | Apparent Shear Strength (ksi) |
|---|---|---|
| EA 9394 | Carbon | 1.354 |
| | Glass | 1.126 |
| EA 9628 | Carbon | 1.468 |
| | Glass | 1.377 |

### 5.1.3 Finite Element Results from FRANC2D

Mode mixity values obtained from FRANC2D for the two adhesive types and adherend types are shown in Table 5.3. As discussed in the previous section, load applied to the specimen model was varied in order to investigate the relationship between the load and the corresponding strain energy rate. Curves were developed to depict this behavior for the given adhesive-adherend combinations and are shown in Figures 5.2a and 5.2b.

Table 5.3 Mode mixity values calculated from FRANC2D.

| Adhesive | Adherend | Mode Mixity (%) |
|---|---|---|
| EA 9394 | Carbon | 49 |
| | Glass | 52 |
| EA 9628 | Carbon | 50 |
| | Glass | 52 |

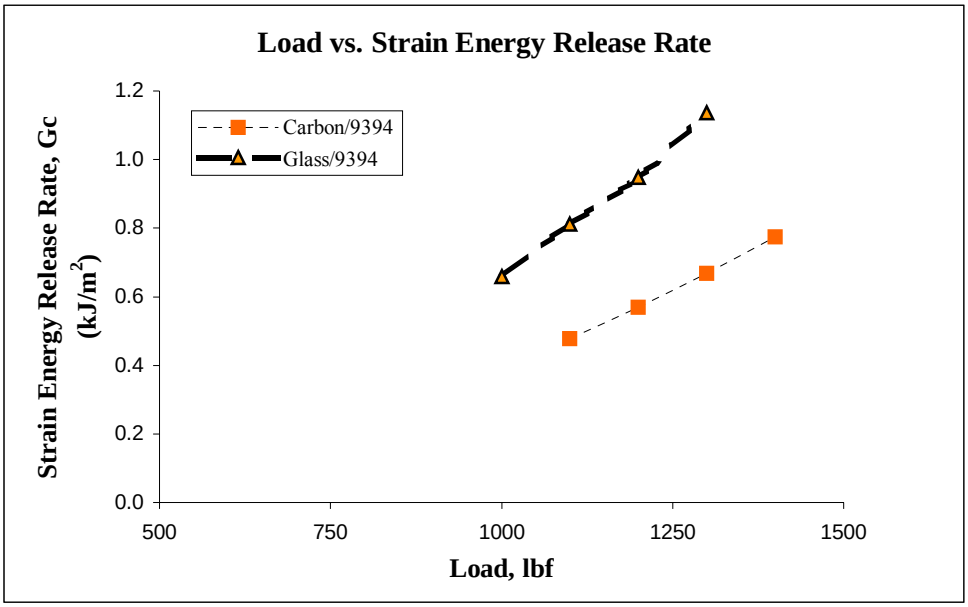


Figure 5.2a Load vs. strain energy release rate for EA 9394 from FRANC2D.

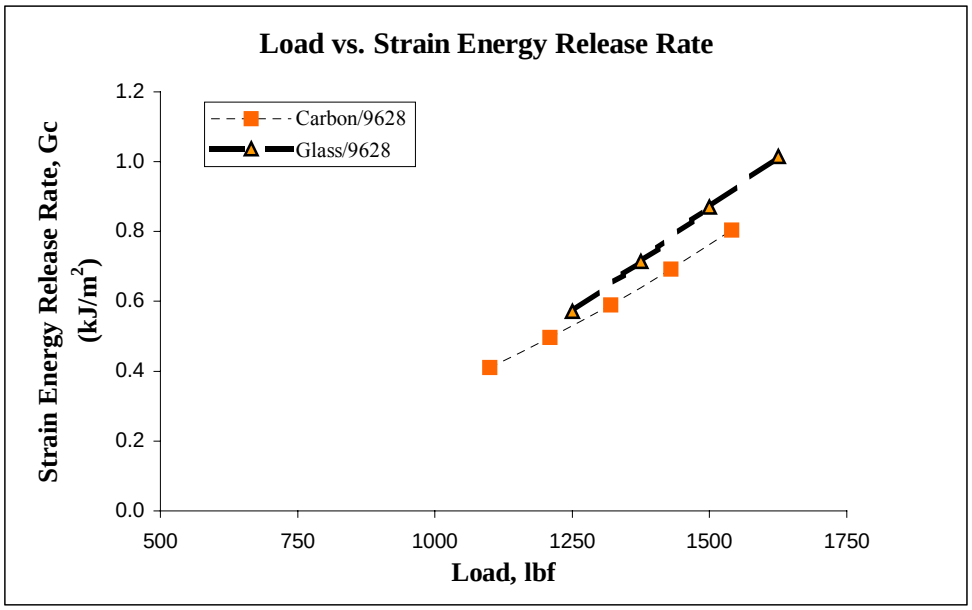


Figure 5.2b Load vs. strain energy release rate for EA 9628 from FRANC2D.

## 5.2 Failure Initiation Prediction

Failure initiation prediction for the single-lap joint specimen configurations was approached by first generating a single mixed-mode fracture toughness curve for each adhesive type. This was achieved by taking the average strain energy rate values for the two composite adherend types used to generate the mode-mixity fracture toughness curve and plotting a single curve for the given adhesive type. As shown in Figures 5.1a and 5.1b, curves generated from glass and carbon adherends coincide with each other for the two adhesive types. However, the curve generated by aluminum adherends is considerably higher than the curves generated by composite adherends. Aluminum was only used with the EA 9493 paste adhesive and considered separately.

Mode-mixity values calculated using FRANC2D for the single-lap joint specimens were plotted on the appropriate adhesive mode-mixity fracture toughness curve to determine the critical strain energy release rate or fracture toughness, as shown in Figures 5.3a and 5.3b. Figure 5.4 illustrates the mode-mixity fracture toughness curve generated using aluminum adherends. Table 5.4 is a summary of the fracture toughness values corresponding to the mode mixities for the given single-lap joint configurations.

The fracture toughness or critical strain energy release rate values obtained were then referred back to the load vs. strain energy release rate curves presented in Figures 5.2a and 5.2b to determine failure load. Figures 5.5a and 5.5b illustrate this step. Corresponding failure load values were then converted to apparent shear strength. Predicted failure values are then compared with the apparent shear strengths obtained experimentally from single-lap joint testing for the two adhesive types as depicted in Figures 5.6a and 5.6b.

## EA 9394 Paste Adhesive

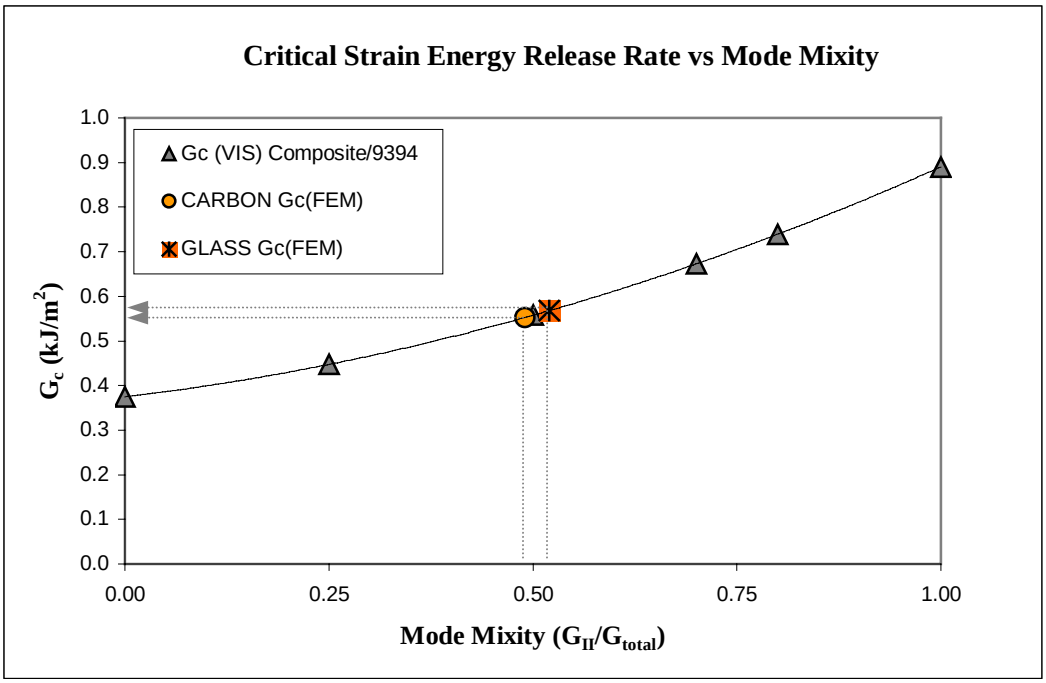


Figure 5.3a $G_C$ predictions for mode mixity values from FRANC2D.

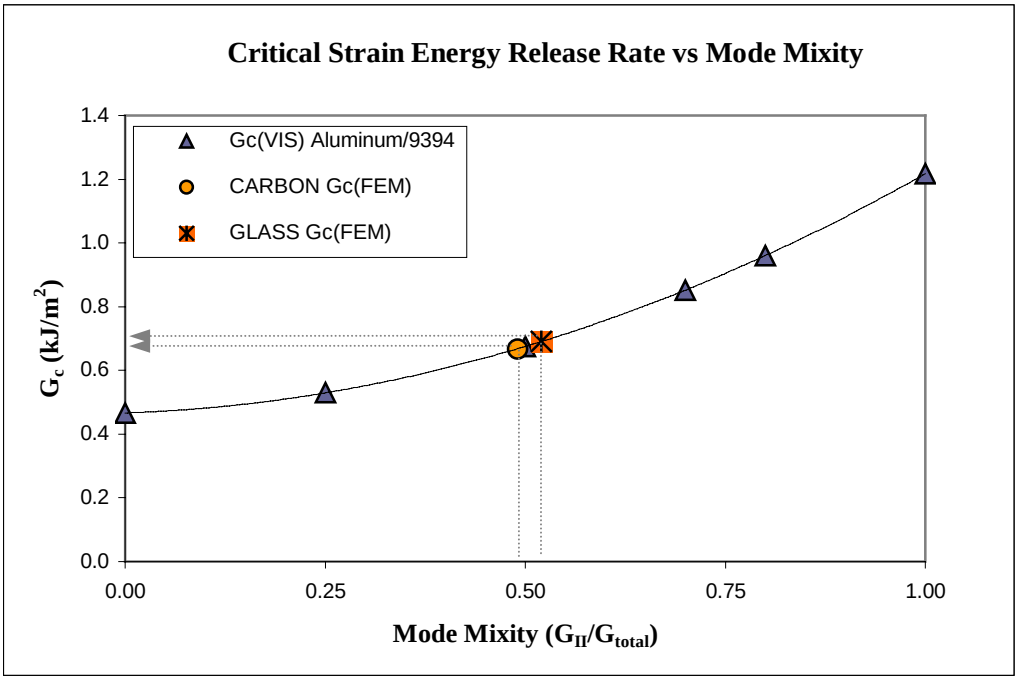


Figure 5.3b $G_C$ predictions for mode mixity values from FRANC2D.

**EA 9628 Film Adhesive**

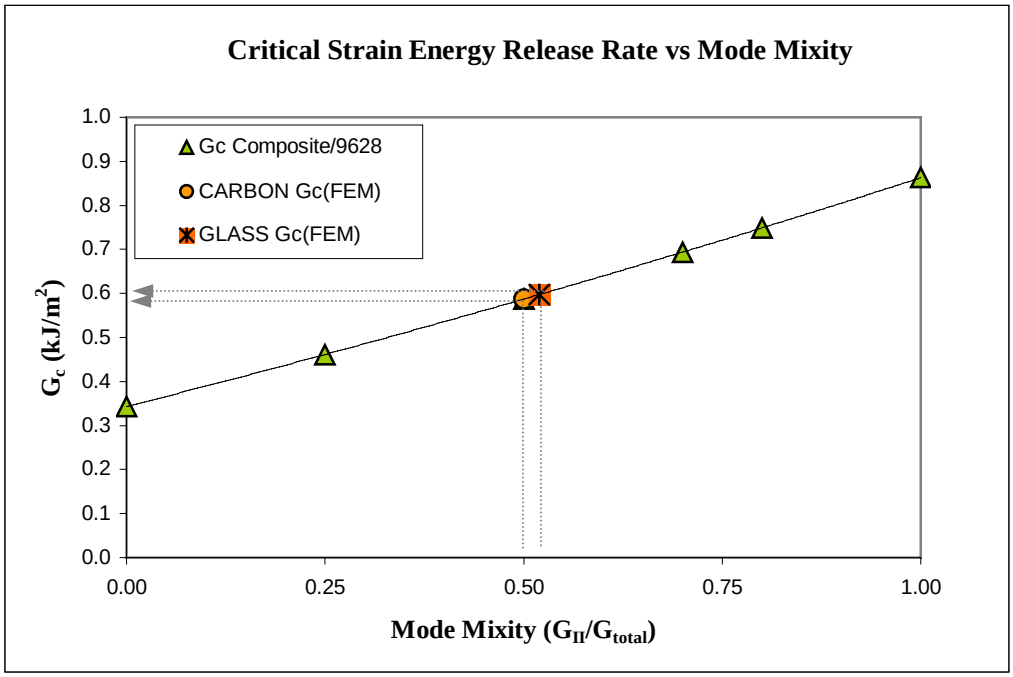


Figure 5.4 $G_C$ predictions for mode mixity values from FRANC2D.

Table 5.4 Summary of the fracture toughness values for corresponding mode mixity.

| Adhesive | Adherend | Mode Mixity (%) | $G_C$ (Comp.) ($kJ/m^2$) | $G_C$ (Aluminum) ($kJ/m^2$) |
|---|---|---|---|---|
| EA 9394 | Carbon | 49 | 0.55 | 0.68 |
| | Glass | 52 | 0.57 | 0.71 |
| EA 9628 | Carbon | 50 | 0.59 | N/A |
| | Glass | 52 | 0.59 | N/A |

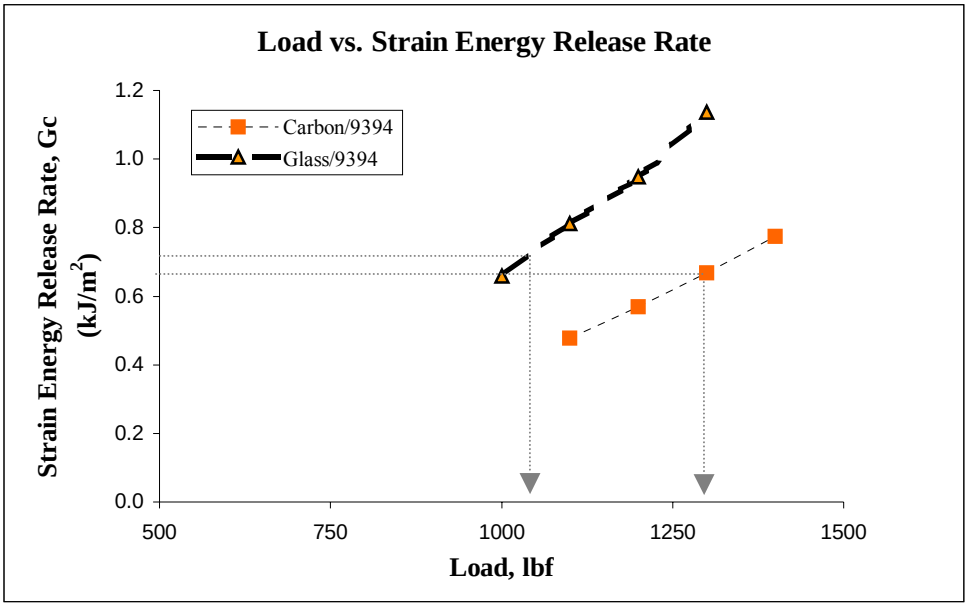


Figure 5.5a Failure load corresponding to $G_C$ predictions from 9394 curve.

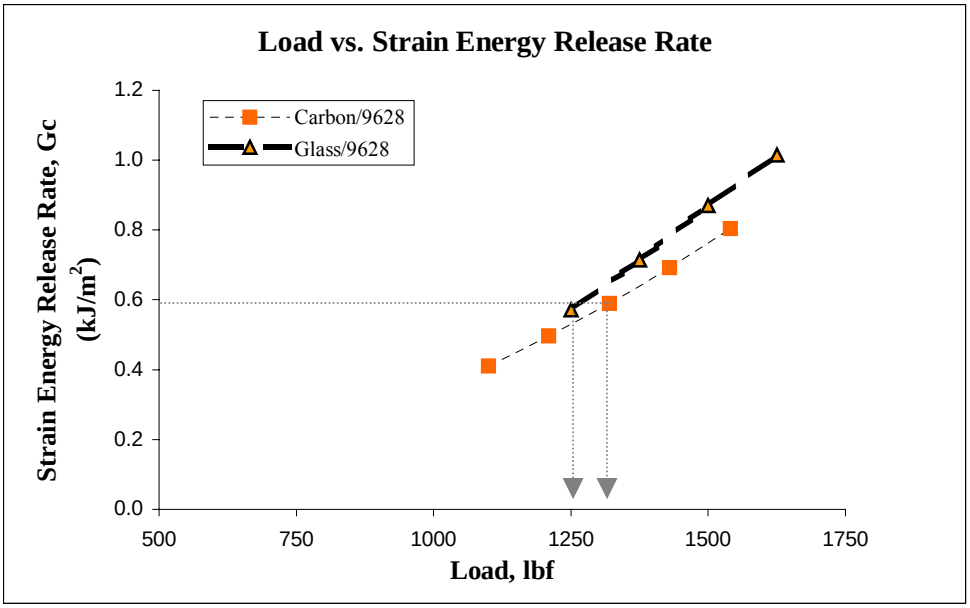


Figure 5.5b Failure load corresponding to $G_C$ predictions from 9628 curve.

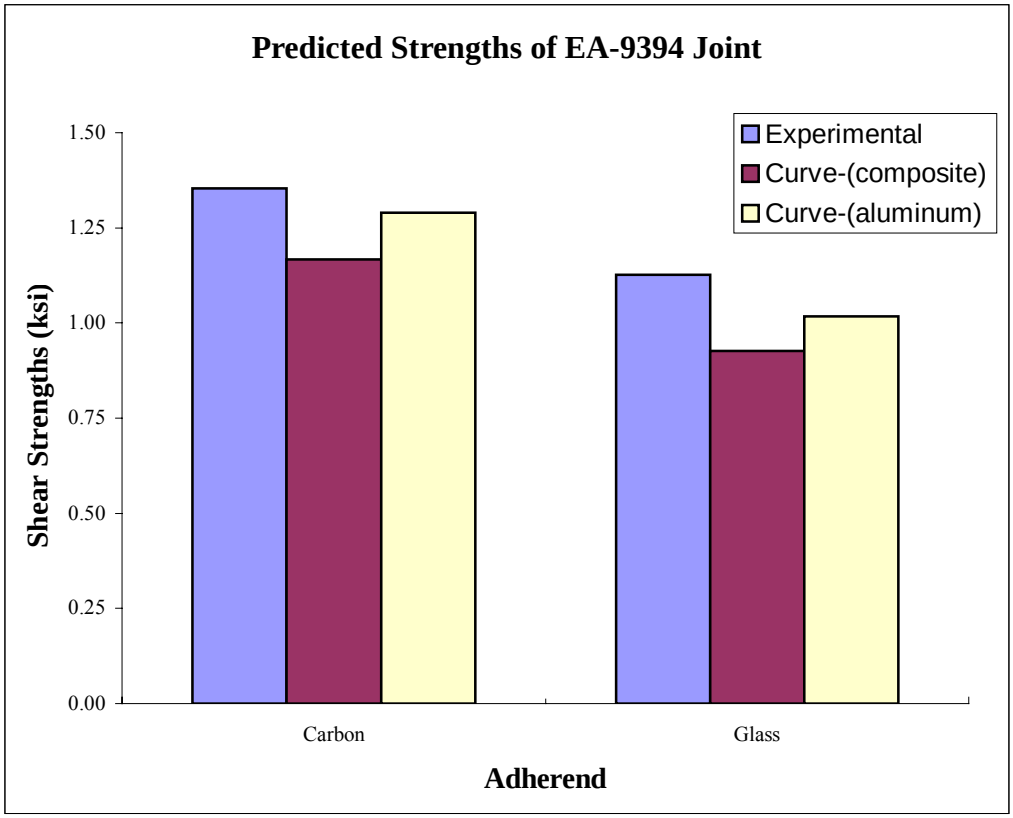


Figure 5.6a Predicted shear strengths and actual shear strengths for EA-9394 single-lap joints.

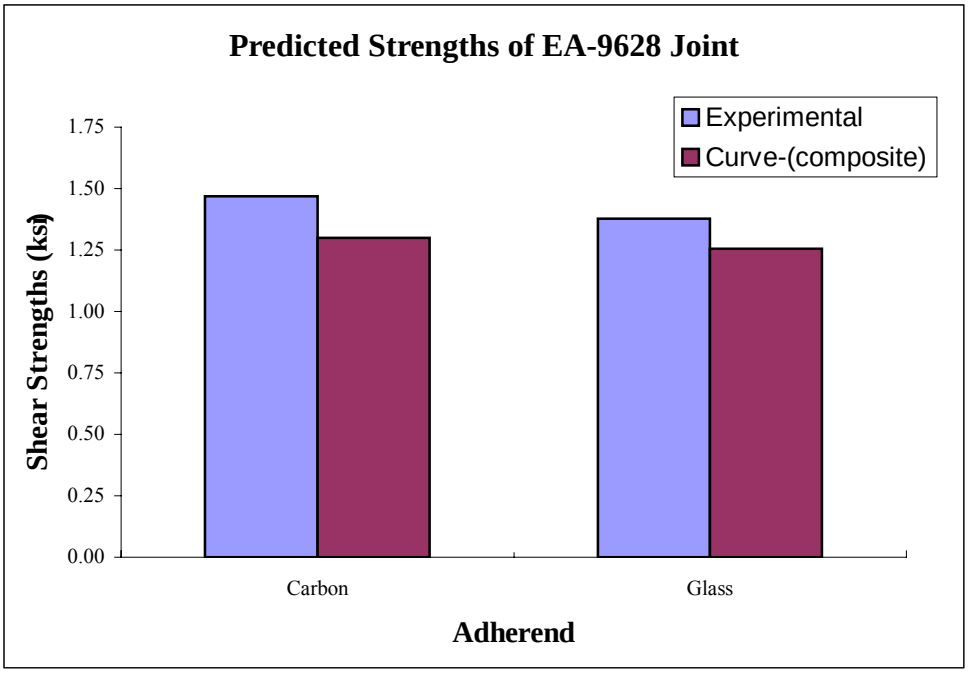


Figure 5.6b Predicted shear strengths and actual shear strengths for EA-9628 single-lap joints.

## 5.3 Discussion

It was observed that mode-mixity fracture toughness curves generated from composite adherends for the two adhesive types coincide with each other. The curve generated for adhesive EA 9394 using aluminum adherends was observed to be slightly higher than the rest and the failure predictions were much closer to the experimental failure values. This is an important observation, suggesting that aluminum adherends are recommended when characterizing an adhesive. Isotropic behavior, a much higher fracture toughness compared to composites and adhesives, and low bending stiffness may be the driving factors behind this effect. Since Aluminum fracture toughness is much higher than adhesive fracture toughness, it is guaranteed to have a cohesive failure, assuming a good bond. On the other hand, composite adherend fracture toughness could be lower than that of adhesive resulting in adherend failure. In this investigation, only carbon-epoxy/9394 and aluminum/9394 specimens showed continuous cohesive failure, while all other specimen configurations showed only initial cohesive failure that soon transformed to adherend failure.

### 5.3.1 Utilization of Mixed-Mode Fracture Toughness Curve

Goal of the mode mixity vs. energy release rate curve developed is to be able to estimate the failure load of a cohesive crack initiation, given the mode mixity. Figure 5.7 summarizes the steps involved in this process. Figure 5.8 summarizes the steps used to utilize the mixed-mode fracture toughness curve method proposed in this investigation to predict a single-lap joint failure load.

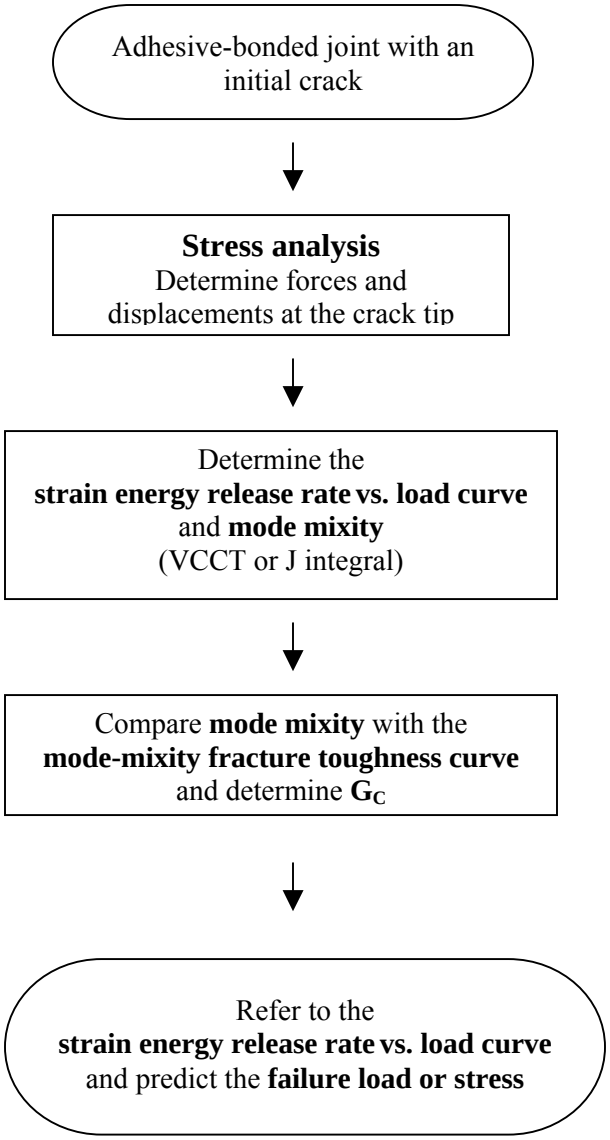


Figure 5.7 Flow chart summarizing the steps to utilize proposed methodology.

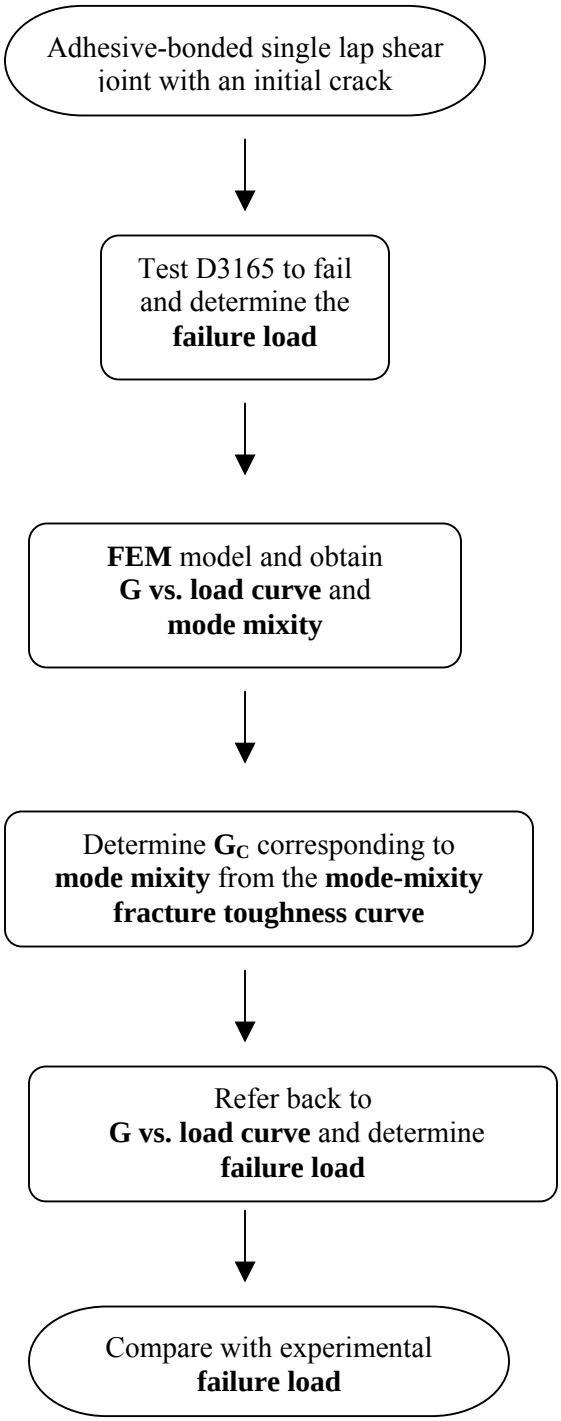


Figure 5.8 Flow chart summarizing the approach to verify the proposed methodology.

# CHAPTER 6

# CONCLUSIONS AND RECOMMENDATIONS

Several conclusions were drawn from this investigation ranging from the process stage and testing methods to the analysis, summarizing the entire investigation. Recommendations were made based on the conclusions with the intention of serving as a stepping-stone for future work related to mixed-mode fracture toughness of adhesives.

## 6.1 Conclusions

- Two types of adhesives—EA9394 paste adhesive and EA9628 film adhesive—were selected for the investigation, based on their wide use in the industry.
- Three types of adherends were selected: Aluminum 2024-T3, Carbon-epoxy, and E-glass. Composite adherends selection was based on their wide use in the industry as adherends in single-lap adhesive joint testing, while Aluminum was selected to study the effect of adherend types on adhesive characterization.
- Mode I and mixed-mode testing were conducted per ASTM D5528 and D6671 standards, while mode II testing was conducted using a three-point bend per SACMA standard.
- Mixed-mode bending test suggested by the ASTM standard for mixed-mode fracture toughness was somewhat inconvenient to use at higher mode mixities, since the hinges that are bonded to the specimen attaching the fixture tend to fail the bonded composite layer of the adherend because of the high load.
- Mixed-mode fracture toughness curves were generated for adhesives EA 9394 and EA 9628. Curves generated using two composite adherends for the two adhesive

types were fairly consistent with each other, while the curve generated from aluminum adherend was slightly higher.

- Adhesive-bonded single-lap shear specimens were tested per ASTM D3165 standard with the two composite adherends selected for the two adhesive types to obtain the failure loads that can be used to compare with predictions made by the proposed method via a mixed-mode fracture toughness curve.
- Adherend failure was observed in all single-lap shear specimens tested. However, failure initiation was determined to be cohesive. Hence, FEM analysis was conducted on a cohesive crack initiation.
- FRANC2D was used as the main analysis code since it was freely available and has been used successfully for fracture analysis.
- J integral was used in FRANC2D to determine the strain energy release rates at the crack tip for the applied load. Load vs. strain energy release rate curves were developed ranging the applied load and calculating the corresponding strain energy release.
- Failure loads obtained experimentally were about 15% off from those predicted by the curves generated using composite adherends.
- Failure loads obtained experimentally were about 5% off from those predicted by the response curves generated using aluminum adherends. Aluminum adherends were only used to generate a curve for EA 9394 paste adhesive.
- Utilization of the proposed methodology based on the mode-mixity fracture toughness curve for certain adhesives is summarized, followed by a conformation using a single-lap joint.

## 6.2 Recommendations for Future Work

- Approach adherend selection keeping in mind the fracture toughness of both the adhesive and adherend, allowing them to, not only initiate cohesively but also propagate cohesively since fracture toughness varies with crack length.
- Use aluminum 20224-T3 adherends with an anodized surface, which proved to be the choice for adhesive characterization to develop curves as opposed to composite adherends.
- Explore alternate testing methods for mixed-mode fracture toughness determination.
- Generate more data points along the response curve to offset the irregularities and to make the curve more accurate.
- Extend FEM analysis to confirm the mode-mixity fracture toughness curves generated experimentally.
- Use a high-end FEM software package for generating the load vs. strain energy release rate curves to compliment the mode-mixity fracture toughness curves developed experimentally.
- Extend the proposed methodology to different environmental conditions and compare this to the environmental effects on the proposed methodology.
- Investigate crack initiation by fatigue effect; compare the mixed-mode fracture toughness curves generated with those by static loading.
- Explore the effect of initial crack length on strain energy release rate at crack tip using FEM analysis.
- Further explore the relationship between load and strain energy release rate maybe further explored by extending the curves generated from FEM model, looking for a possible trend.

# REFERENCES

[1] "Primary Adhesively Bonded Structure Technology (PABST) Industry Review", Page 166-204, September 14-16, 1977.

[2] Ullah, Md. H., "Analysis of Cohesive Failure of Adhesive Bonded Composite Joints", M.S. Thesis, Dept. of Mechanical Engineering, Wichita State University, Wichita, KS, USA, 2002.

[3] "Standard Test Method for Strength Properties of Adhesives in Shear by Tension Loading of Single Lap Joint Laminated Assemblies", *Annual Book of ASTM Standards*, 2000, Vol. 15.06 [CD-ROM].

[4] Ramaswamy, S. and Tippur, H. V. and Xu, L., "Mixed mode Fracture Deformations Studied Using A Modified Flexural Specimen and Coherent Gradient Sensing", *Experimental Mechanics, SAGE Social Science Collection,* Sept. 1993.

[5] Kossira, H. and Weerts, U, "Mixed Mode Fracture Characterization of Adhesive Joints", International Council of Aeronautical Science, 2000

[6] Pirondi, A. and Nicoletto, G., "Mixed Mode Fracture Envelope of a Structural Adhesive", Department of Industrial Engineering, University of Parma, Italy, June 2001.

[7] Nairn, A. J., "Energy Release Rate Analysis for Adhesive and Laminate Double Cantilever Beam specimens emphasizing the effect of residual stresses", *International Journal of Adhesion & Adhesives*, Vol. 20, 1999, pp 59-70.

[8] Moore, D.R. and Williams J. G., "A Protocol for Determination of the Adhesive Fracture Toughness by Peel Testing of Flexible Laminates", June 2000, URL: http://www3.imperial.ac.uk/pls/portallive/docs/1/41494.pdf [cited 12 December 2004].

[9] Yang, Q. D., Thouless, M. D. and Ward, S. M., "Elastic-Plastic Mode-II Fracture of Adhesive Joints", May 2000, URL: http://www-personal.engin.umich.edu/~thouless/Mode2.pdf [cited 15 Dec. 2004].

[10] Krueger, R., "A Shell/3D Modeling Technique for Delaminations in Composite Laminates", *Proceedings of the American Society for Composites, 14th Technical Conference*, Technomic Publishing, ISBN 1-56676-791-1, pp. 843-852, 1999.

[11] Bardis, J. D. and Kedward, K. T., "Surface Preparation Effects on Mode I Testing of Adhesively Bonded Composite Joints", *Journal of Composite Technology and Research*, Vol. 24, Issue 1, Jan. 2002.

[12] "Standard Method for Mixed Mode I-Mode II Interlaminar Fracture Toughness of Unidirectional Fiber Reinforced Polymer Matrix Composites", *Annual Book of ASTM Standards*, Vol. 15.06, 2001 [CD-ROM].

[13] Hashemi, S., Kinloch, A. J. and Williams, G., "Mixed-Mode Fracture in Fiber- Polymer Composite Laminates", *Composite Materials: Fatigue and Fracture,* ASTM STP 1110, 1999.

[14] Anderson, T. L., "Fracture Mechanics: Fundamentals and Applications", 2nd edition, CRC Press, pp. 44-46, 1995.

[15] "Standard Test Method for Mode I Interlaminar Fracture Toughness of Unidirectional Fiber-Reinforced Polymer Matrix Composites", *Annual Book of ASTM Standards*, Vol. 15.06, 2001 [CD-ROM].

[16] "Standard Test Method for Mode II Interlaminar Fracture Toughness of Unidirectional Fiber-Reinforced Polymer Matrix Composites", SACMA BMS 8-276F, 2000.

[17] Huang, H., Yang, C., Tomblin, J. and Harter, P., "Stress and Failure Analysis of Adhesive-Bonded Composite Joints using ASTM D3165 Specimens" *Journal of Composites Technology and Research* Vol. 24, Issue 2, April 2002.

[18] Cope, D. A., Lacy, T. E., "Modeling Mechanical Fasteners in Lap Joints for Stress Intensity Determination", Joint Council on Aging Aircraft, *Aging Aircraft Conference*, 2000.

[19] B-Basis Design Allowables for Epoxy-Based Prepreg, *Advanced General Aviation Transport Experiments (AGATE)*, 2001 URL: http://www.niar.wichita.edu/agate [cited 10 Oct. 2005].

[20] Reeder, R. J and Crews, R. Jr., "Mixed mode Bending Method for Delamination Testing", *AA Journal*, Vol. 28, Number 7, pp. 1270-1276, July 1990.

[21] Guess, T. R., Reedy, Stavig, M. E., "Mechanical Properties of Hysol EA-9394 Structural Adhesive", *Sandia Report, SAND95-0229,* Feb. 1995.

# APPENDIX

# APPENDIX A

# EXPERIMENTAL DATA

## Mode I

Table A.1 Mode I critical strain energy release rate values for Al/9394

| Specimen Name | $G_C$ ($kJ/m^2$) |
|---|---|
| MIAL21 | N/A |
| MIAL22 | N/A |
| MIAL23 | 0.459 |
| MIAL24 | 0.422 |
| MIAL25 | 0.435 |
| MIAL26 | 0.369 |

Table A.2 Mode I critical strain energy release rate values for carbon/9628

| Specimen Name | $G_C$ ($kJ/m^2$) |
|---|---|
| MIC11 | 0.358 |
| MIC12 | 0.403 |
| MIC13 | 0.320 |
| MIC14 | N/A |
| MIC15 | 0.316 |

Table A.3 Mode I critical strain energy release rate values for carbon/9394

| Specimen Name | $G_C$ ($kJ/m^2$) |
|---|---|
| MIC21 | 0.433 |
| MIC22 | 0.360 |
| MIC23 | 0.238 |
| MIC24 | 0.291 |
| MIC25 | 0.273 |
| MIC26 | 0.478 |

Table A.4 Mode I critical strain energy release rate values for glass/9628

| Specimen Name | $G_C$ ($kJ/m^2$) |
|---|---|
| MIF11 | 0.322 |
| MIF12 | 0.332 |
| MIF13 | 0.328 |
| MIF14 | 0.419 |
| MIF15 | 0.292 |

Table A.5 Mode I critical strain energy release rate values for glass/9394

| Specimen Name | $G_C$ ($kJ/m^2$) |
|---|---|
| MIF21 | 0.421 |
| MIF22 | 0.500 |
| MIF23 | 0.399 |
| MIF24 | 0.397 |
| MIF25 | 0.407 |

**Mixed Mode 25%**

Table A.6 Mixed Mode 25% critical strain energy release rate values for Aluminum/9394

| Specimen Name | $G_C$ ($kJ/m^2$) |
|---|---|
| MMB25AL21 | N/A |
| MMB25AL22 | 0.455 |
| MMB25AL23 | 0.341 |
| MMB25AL24 | 0.420 |
| MMB25AL25 | N/A |

Table A.7 Mixed Mode 25% critical strain energy release rate values for carbon/9628

| Specimen Name | $G_C$ ($kJ/m^2$) |
|---|---|
| MMB25C11 | N/A |
| MMB25C12 | 0.455 |
| MMB25C13 | 0.341 |
| MMB25C14 | 0.436 |
| MMB25C15 | N/A |

Table A.8 Mixed Mode 25% critical strain energy release rate values for carbon/9394

| Specimen Name | $G_C$ ($kJ/m^2$) |
|---|---|
| MMB25C21 | N/A |
| MMB25C22 | 0.455 |
| MMB25C23 | 0.341 |
| MMB25C24 | 0.436 |
| MMB25C25 | N/A |

Table A.9 Mixed Mode 25% critical strain energy release rate values for glass/9628

| Specimen Name | $G_C$ ($kJ/m^2$) |
|---|---|
| MMB25F11 | 0.609 |
| MMB25F12 | N/A |
| MMB25F13 | 0.293 |
| MMB25F14 | N/A |
| MMB25F15 | 0.597 |

Table A.10 Mixed Mode 25% critical strain energy release rate values for glass/9394

| Specimen Name | $G_C$ ($kJ/m^2$) |
|---|---|
| MMB25F21 | N/A |
| MMB25F22 | 0.282 |
| MMB25F23 | 0.345 |
| MMB25F24 | 0.455 |
| MMB25F25 | 0.429 |

**Mixed Mode 50%**

Table A.11 Mixed Mode 50% critical strain energy release rate values for Aluminum/9394

| Specimen Name | $G_C$ ($kJ/m^2$) |
|---|---|
| MMB40AL21 | N/A |
| MMB40AL22 | 0.555 |
| MMB40AL23 | 0.698 |
| MMB40AL24 | 0.732 |
| MMB40AL25 | 0.664 |
| MMB40AL26 | 0.612 |

Table A.12 Mixed Mode 50% critical strain energy release rate values for carbon/9628

| Specimen Name | $G_C$ ($kJ/m^2$) |
|---|---|
| MMB25C11 | N/A |
| MMB25C12 | N/A |
| MMB25C13 | N/A |
| MMB25C14 | 0.430 |
| MMB25C15 | 0.569 |
| MMB25C16 | 0.619 |

Table A.13 Mixed Mode 50% critical strain energy release rate values for carbon/9394

| Specimen Name | $G_C$ ($kJ/m^2$) |
|---|---|
| MMB50C21 | 0.666 |
| MMB50C22 | 0.683 |
| MMB50C23 | 0.514 |
| MMB50C24 | NA |
| MMB50C25 | 0.538 |

Table A.14 Mixed Mode 50% critical strain energy release rate values for glass/9628

| Specimen Name | $G_C$ ($kJ/m^2$) |
|---|---|
| MMB50F11 | N/A |
| MMB50F12 | 0.678 |
| MMB50F13 | 0.542 |
| MMB50F14 | 0.542 |
| MMB50F15 | 0.661 |

Table A.15 Mixed Mode 50% critical strain energy release rate values for glass/9394

| Specimen Name | $G_C$ ($kJ/m^2$) |
|---|---|
| MMB50F21 | 0.539 |
| MMB50F22 | 0.757 |
| MMB50F23 | 0.686 |
| MMB50F24 | 0.639 |
| MMB50F25 | 0.666 |

**Mixed Mode 70%**

Table A.16 Mixed Mode 70% critical strain energy release rate values for carbon/9394

| Specimen Name | $G_C$ ($kJ/m^2$) |
|---|---|
| MMB70C21 | N/A |
| MMB70C22 | 0.725 |
| MMB70C23 | 0.626 |
| MMB70C24 | 0.720 |
| MMB70C25 | N/A |
| MMB70C26 | 0.647 |

Table A.17 Mixed Mode 70% critical strain energy release rate values for glass/9628

| Specimen Name | $G_C$ ($kJ/m^2$) |
|---|---|
| MMB70F11 | 0.678 |
| MMB70F12 | 0.627 |
| MMB70F13 | 0.669 |
| MMB70F14 | N/A |
| MMB70F15 | 0.723 |

Table A.18 Mixed Mode 70% critical strain energy release rate values for glass/9394

| Specimen Name | $G_C$ ($kJ/m^2$) |
|---|---|
| MMB70F21 | 0.792 |
| MMB70F22 | N/A |
| MMB70F23 | N/A |
| MMB70F24 | N/A |
| MMB70F25 | 0.683 |
| MMB70F26 | 0.619 |

**Mixed Mode 80%**

Table A.19 Mixed Mode 80% critical strain energy release rate values for Aluminum/9394

| Specimen Name | $G_C$ ($kJ/m^2$) |
|---|---|
| MMB80AL21 | 0.912 |
| MMB80AL22 | N/A |
| MMB80AL23 | 0.676 |
| MMB80AL24 | 0.740 |
| MMB80AL25 | 0.790 |
| MMB80AL26 | 0.735 |

Table A.20 Mixed Mode 80% critical strain energy release rate values for carbon/9628

| Specimen Name | $G_C$ ($kJ/m^2$) |
|---|---|
| MMB80C11 | 0.671 |
| MMB80C12 | 0.814 |
| MMB80C13 | N/A |
| MMB80C14 | 0.929 |
| MMB80C15 | N/A |

Table A.21 Mixed Mode 80% critical strain energy release rate values for carbon/9394

| Specimen Name | $G_C$ ($kJ/m^2$) |
|---|---|
| MMB80C21 | N/A |
| MMB80C22 | 0.529 |
| MMB80C23 | 0.584 |
| MMB80C24 | N/A |
| MMB80C25 | 0.696 |
| MMB80C26 | 0.713 |

Table A.22 Mixed Mode 80% critical strain energy release rate values for glass/9394

| Specimen Name | $G_C$ ($kJ/m^2$) |
|---|---|
| MMB80F21 | 0.667 |
| MMB80F22 | 0.601 |
| MMB80F23 | 0.621 |
| MMB80F24 | 0.657 |
| MMB80F25 | 0.623 |

**Mode II**

Table A.23 Mode II critical strain energy release rate values for Aluminum/9394

| Specimen Name | $G_C$ ($kJ/m^2$) |
|---|---|
| MIIAL21 | 0.990 |
| MIIAL22 | 1.044 |
| MIIAL23 | 1.098 |
| MIIAL24 | 1.272 |
| MIIAL25 | 1.273 |
| MIIAL26 | 1.133 |

Table A.24 Mode II critical strain energy release rate values for carbon/9628

| Specimen Name | $G_C$ ($kJ/m^2$) |
|---|---|
| MIIC11 | 0.717 |
| MIIC12 | 0.762 |
| MIIC13 | 0.916 |
| MIIC14 | 1.106 |
| MIIC15 | 0.966 |

Table A.25 Mode II critical strain energy release rate values for glass/9628

| Specimen Name | $G_C$ ($kJ/m^2$) |
|---|---|
| MIIF11 | 0.831 |
| MIIF12 | 0.817 |
| MIIF13 | 0.746 |
| MIIF14 | 0.817 |
| MIIF15 | 0.794 |

Table A.26 Mode II critical strain energy release rate values for carbon/9394

| Specimen Name | $G_C$ ($kJ/m^2$) |
|---|---|
| MIIC21 | 1.078 |
| MIIC22 | 0.894 |
| MIIC23 | 0.801 |
| MIIC24 | 0.802 |
| MIIC25 | 0.658 |
| MIIC26 | 0.770 |

Table A.27 Mode II critical strain energy release rate values for glass/9394

| Specimen Name | $G_C$ ($kJ/m^2$) |
|---|---|
| MIIF21 | 1.025 |
| MIIF22 | 0.853 |
| MIIF23 | 0.915 |
| MIIF24 | 0.941 |
| MIIF25 | 0.794 |

**Single-Lap Joint Data (D3165)**

Table A.28 Single-lap joint failure loads for carbon/9628

| Specimen Name | Width (in) | Overlap Length (in) | Max. Load (lbf) | Shear Strength (ksi) |
|---|---|---|---|---|
| SLSC11 | 1.018 | 0.984 | 1472 | 1.470 |
| SLSC12 | 1.017 | 0.985 | 1442 | 1.441 |
| SLSC13 | 1.016 | 1.000 | 1507 | 1.484 |
| SLSC14 | 1.016 | 1.018 | 1393 | 1.347 |
| SLSC15 | 1.019 | 1.020 | N/A | N/A |
| SLSC16 | 1.016 | 0.990 | 1607 | 1.597 |

Table A.29 Single-lap joint failure loads for carbon/9394

| Specimen Name | Width (in) | Overlap Length (in) | Max. Load (lbf) | Shear Strength (ksi) |
|---|---|---|---|---|
| SLSC21 | 1.017 | 1.024 | 1480 | 1.421 |
| SLSC22 | 1.017 | 1.028 | 1400 | 1.339 |
| SLSC23 | 1.016 | 1.029 | 1333 | 1.275 |
| SLSC24 | 1.018 | 1.027 | 1424 | 1.362 |
| SLSC25 | 1.020 | 1.023 | 1396 | 1.339 |
| SLSC26 | 1.020 | 1.031 | 1460 | 1.388 |

Table A.30 Single-lap joint failure loads for glass/9628

| Specimen Name | Width (in) | Overlap Length (in) | Max. Load (lbf) | Shear Strength (ksi) |
|---|---|---|---|---|
| SLSF11 | 1.016 | 1.020 | 1306 | 1.549 |
| SLSF12 | 1.019 | 1.020 | 1452 | 1.688 |
| SLSF13 | 1.017 | 1.028 | N/A | N/A |
| SLSF14 | 1.019 | 1.033 | 1374 | 1.590 |
| SLSF15 | 1.017 | 1.033 | 1464 | 1.775 |
| SLSF16 | 1.016 | 1.018 | 1444 | 1.784 |

Table A.30 Single-lap joint failure loads for glass/9628

| Specimen Name | Width (in) | Overlap Length (in) | Max. Load (lbf) | Shear Strength (ksi) |
|---|---|---|---|---|
| SLSF21 | 1.016 | 0.987 | 1068 | 1.065 |
| SLSF22 | 1.019 | 0.984 | 1152 | 1.149 |
| SLSF23 | 1.018 | 0.978 | 1116 | 1.121 |
| SLSF24 | 1.018 | 0.982 | N/A | N/A |
| SLSF25 | 1.019 | 0.986 | 1152 | 1.148 |
| SLSF26 | 1.020 | 0.989 | 1156 | 1.147 |